IDŐJÁRÁS

QUARTERLY JOURNAL
OF THE HUNGARIAN METEOROLOGICAL SERVICE

CONTENTS

****

http://www.met.hu/firat/ido-e.html

VOL. 102 * NO. 4 * OCTOBER–DECEMBER 1998

IDŐJÁRÁS

Quarterly Journal of the Hungarian Meteorological Service

Editorial Office: P.O. Box 39, H-1675 Budapest, Hungary or
Gilice tér 39, H-1181 Budapest, Hungary
E-mail: gmajor@met.hu or *antal@met.hu*
Fax: (36-1) 290-7387

Subscription by

mail: IDŐJÁRÁS, P.O. Box 39, H-1675 Budapest, Hungary;
E-mail: gmajor@met.hu or *antal@met.hu*; *Fax: (36-1) 290-7387*

IDŐJÁRÁS

Quarterly Journal of the Hungarian Meteorological Service
Vol. 102, No. 4, October–December 1998, pp. 201–218

Statistical estimate of the vertical ozone structure

D. Spänkuch and **E. Schulz**

Meteorological Observatory Potsdam, German Weather Service
Postfach 60 05 52, D-14405 Potsdam, Germany
E-mail: spaenkuch@mop.dwd.d400.de

(Manuscript received 1 June 1998; in final form 28 September 1998)

Abstract—A multiple linear regression approach is presented to estimate layer ozone amount $\Delta\Omega$ from predictors accessible from model outputs of meteorological analysis and prediction additionally to the total ozone amount that has regularly been monitored from satellites for several years. Total column ozone is the most important predictor, in general, of the approach developed and checked for northern midlatidudes. The second most important predictor is the thermal state of atmospheric layers. The accuracy of the statistical estimate is assessed to be about 3 to 10 per cent in maximum depending on atmospheric layer and season. Comparison of the estimate with more than one hundred ozone sonde data at Hohenpeissenberg, Germany, throughout one year showed promising results between 300 and 50 hPa when outliers of about 8 to 10 per cent of cases are omitted. The outliers were mainly found for the layer between 200 to 100 hPa and are obviously related to filament-like structures in ozone there. The most satisfying results were obtained for the tropopause region 300–200 hPa with a reduction of variance of about 0.7 to 0.8. This altitude range is the most difficult one for monitoring from satellites.

Key-words: stratospheric ozone, forecasting, multiple linear regression.

1. Introduction

Atmospheric ozone has been a permanent issue for many years because of its harmful effects to the environment. Understanding the atmospheric ozone cycle and its change needs inter alia a detailed knowledge of the ozone distribution in space and time. Our current knowledge on the atmospheric ozone distribution, its variability and long-term variations and trends relies on data sources of different characteristics and quality (e.g., *WMO*, 1995). Satellites have monitored globally total column ozone Ω and the vertical ozone distribution of the upper and middle stratosphere since the late seventies. Information on the ozone profile from satellites are gained from backscattered radiation in the UV

between 252 and 306 nm by the Solar Backscatter Ultraviolet Spectrometer (SBUV) and solar occultation absorption measurements around 600 nm by the Stratospheric Aerosol and Gas Experiment (SAGE I and II). Limb emission measurements at 9.6 μm are anticipated with the Michelson Interferometric Passive Atmosphere Sounder (MIPAS) on ENVISAT. Occultation and limb measurements exhibit in general high vertical resolution down to the tropopause. The vertical resolution of SBUV data is about 8 km above 25 km altitude and increases to 15 km below that level. Intercomparisons between SAGE II and SBUV results made in the interval 1984 to 1990 agreed to better than 5% in general (*WMO*, 1995).

The first information on the vertical ozone structure, although of limited resolution, was drawn from Umkehr observations (*Götz*, 1931). Ozonesondes having high vertical resolution up to the bursting level of balloons at about 30 km altitude have been launched since the midsixties. Ozone lidars of high vertical resolution per se have been in operation since the late eighties. Stratospheric ozone research needs lidars of sufficient power, however, particularly for the upper stratosphere. All ground-based sounding systems are regionally representative. However, ground-based quasicontinuous monitoring is not feasible because of meteorological (cloudiness for lidars) as well as cost-effective reasons (both profiling systems).

Summarizing the present data situation we state a global data set of sufficient quality since 1979 for the upper stratosphere which will be updated by corresponding satellite launches in the future. Below about 20 km reliable information of sufficient quality can be presently gained only by satellite measurements with tangential observation geometry (SAGE at present) and by ozonesondes and lidars. For the tropopause region which is of particular importance to the role of ozone depletion in radiative forcing of the Earth's climate system (e.g., *Lacis et al.*, 1990; *Ramaswamy et al.*, 1992) and below, the interpretation of occultation and limb measurements is limited in the presence of clouds. Information on ozone variations at these heights are mainly from ozonesondes and lidars. Thus there is a deficit of ozone data in the troposphere and lowermost stratosphere particularly because ozonesonde and lidar measurements are only sporadically available and only regionally representative. Substantial improvement by new satellite systems is not to be expected in the near future.

However, there are some founded reasons for improvement of the data basis situation by using information of other meteorological parameters. Statistical approaches have been used with success to predict total column ozone (e.g., *Burrows et al.*, 1995; *Spänkuch* and *Schulz*, 1995, 1997a; *Long et al.*, 1996) and to check the quality of total column ozone measurements (*Spänkuch* and *Schulz*, 1997b). They are also capable for ascertaining the scope of the climatological vertical ozone structure. The physical background for significant statistical relations between the vertical ozone structure and other meteorological

parameters is given mainly by the dominance of dynamical processes up to the middle stratosphere in building up the vertical ozone structure.The approach of statistical profiling has widely been used in numerous numerical weather prediction schemes in particular to infer the vertical humidity structure. In ozone research, analogous efforts were made to evaluate the quality of Umkehr observations (*de Luisi* and *Mateer*, 1971) and to improve retrievals of satellite measurements (e.g., *Sellers* and *Yarger*, 1969; *Timofeyev et al.*, 1974; *Feister* and *Spänkuch*, 1977), but these approaches have obviously not been applied despite of partly promising results in particular by the last authors.

Any possible improvement of the data basis situation by statistical approaches does not mean, however, a possible replacement of measurements by statistical estimates as they reflect normal situations per se. Statistical approaches, however, have another benefit, too. Outliers are either the results of incorrect measurements or data handling or, that is much more important, they indicate the impact of some not yet recognized or, due to changing environmental conditions, newly acting processes. The history of the detection of the antarctic ozone hole is a good example in this respect (e.g., *Fabian*, 1989; *Roan*, 1989).

This paper describes the statistical approach applied to assess the vertical ozone structure in Central Europe and estimates its quality by theoretical considerations as well as by intercomparison with more than 100 ozone sonde data at Hohenpeissenberg, Germany, throughout one year.

2. Short review of the climatology of the vertical ozone structure

Climatology is the bench mark of each statistical approach. Thus some climatological knowledge is needed for a sound assessment of such approaches. This climatological background is given in *Fig. 1* as frequency distribution of layer ozone $\Delta\Omega$ at Hohenpeissenberg for the atmospheric layers indicated in this figure. The frequency distribution is given for normal years in the left panels and for disturbed years after volcanic eruptions (1983, 1992 and 1993) in the right panels. The scale of $\Delta\Omega$ is the same for all layers for easy intercomparison. The frequency distributions are given for the whole year; shorter time intervals (seasons, months) as references result in a narrowing of the distribution and a shift of the characteristic distribution parameters according to the seasonal course (e.g., *Dütsch*, 1978). Additionally, the lowest panels of Fig. 1 give the frequency distribution of total ozone Ω.

Total ozone and layer ozone from 300 to 50 hPa are lognormally or gamma distributed as the result of rare cases of high layer ozone. The distribution is broadest between 200 and 50 hPa with a standard deviation of about 15 to 20 DU and narrowest in the lower and middle troposphere with a standard of about 2 DU, respectively. Normal and disturbed years differ in the location of the

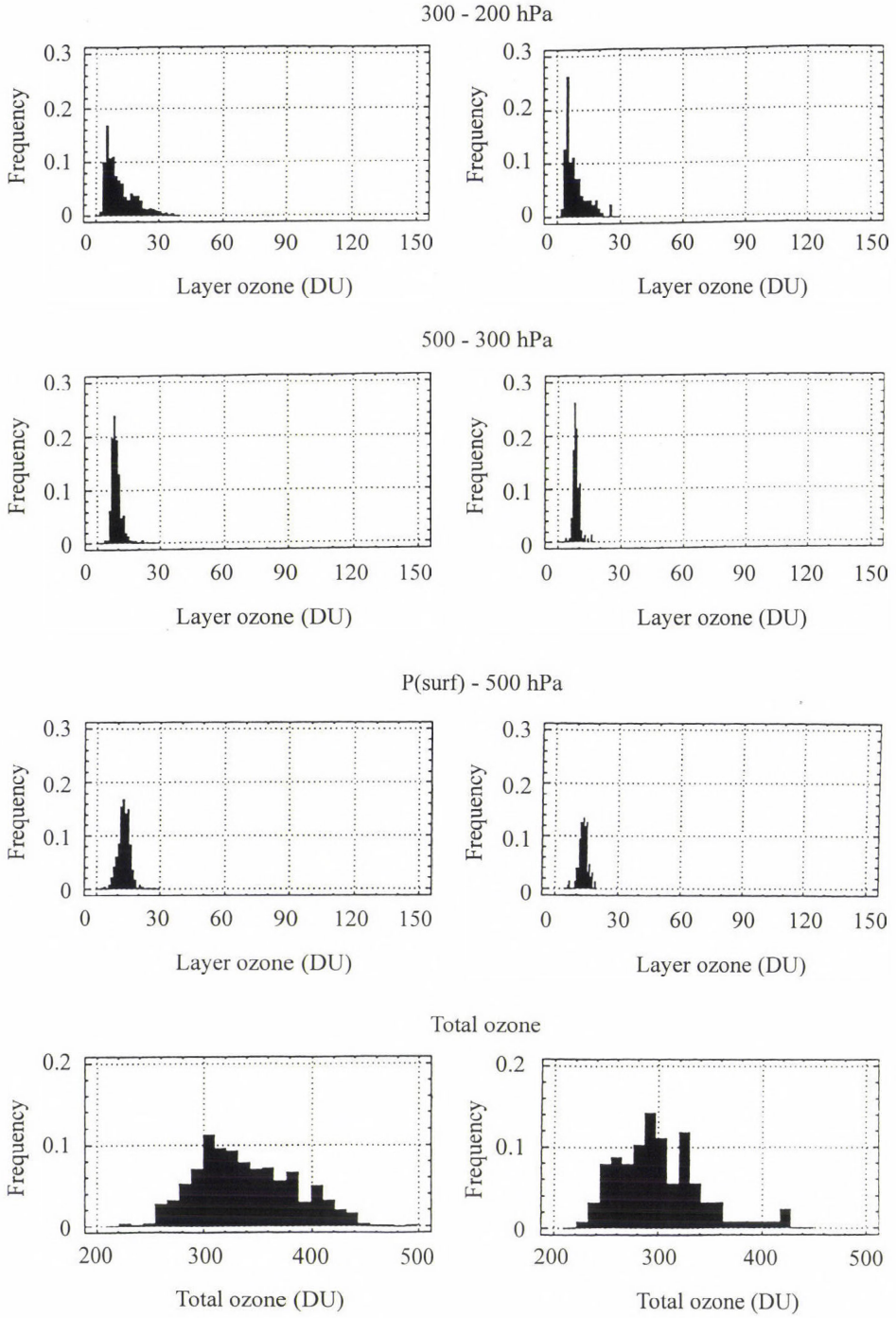
300 - 200 hPa
Frequency
0.3
0.2
0.1
0
0 30 60 90 120 150
Layer ozone (DU)
500 - 300 hPa
P(surf) - 500 hPa
Total ozone
0.2
200 300 400 500
Total ozone (DU)

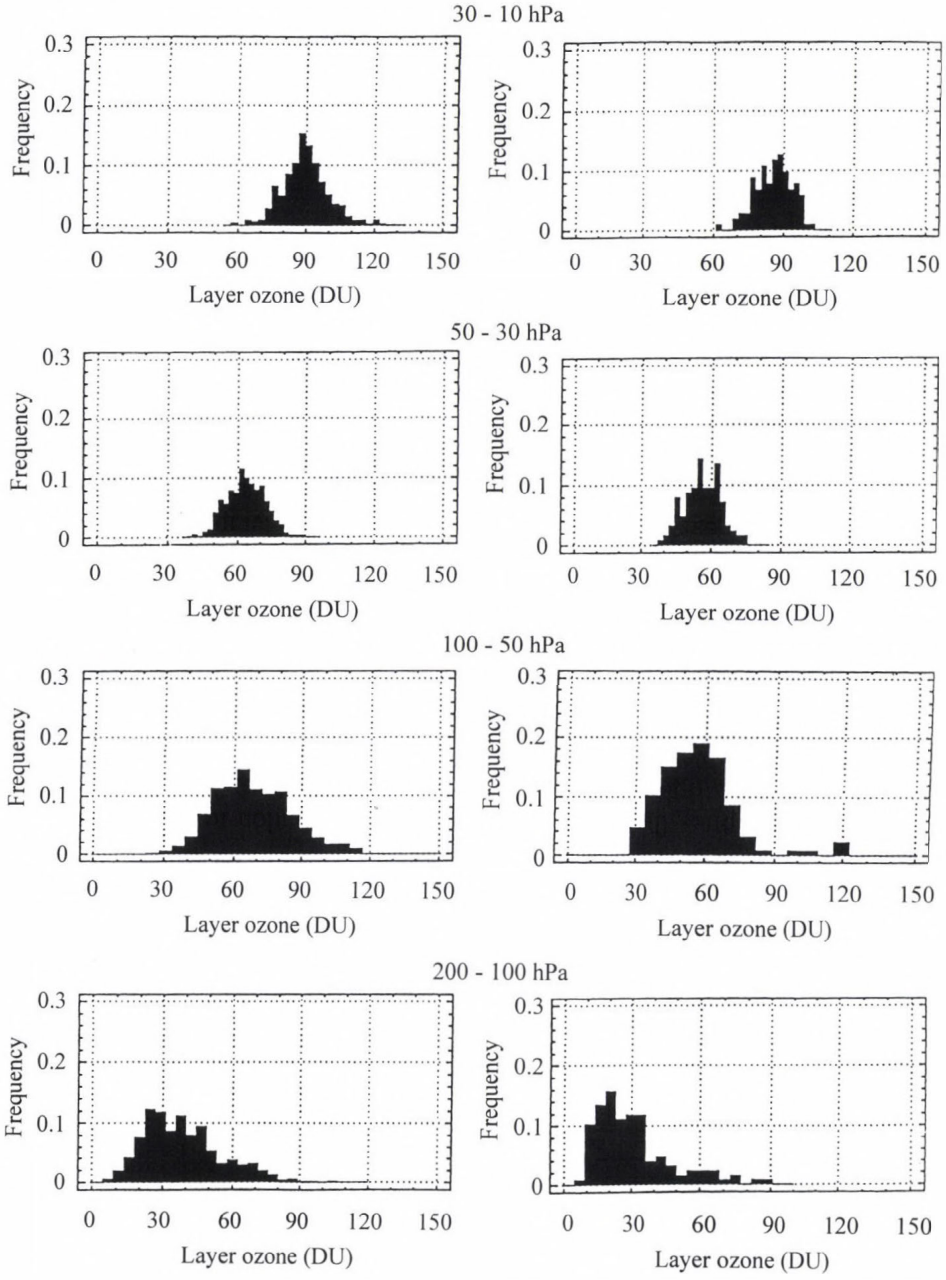

Fig. 1. Frequency distribution of total column ozone (Ω) and layer ozone amount (ΔΩ) at Hohenpeissenberg 1975 to 1994 for undisturbed years (left) and for years after volcanic eruptions (right).

distribution, but not in its spread. *Krzyścin* (1994) has already stated a shift of the Ω frequency distribution as a whole throughout the years without any change of its shape. Fig. 1 shows this finding for $\Delta\Omega$, too. The most reduction in layer ozone after volcanic eruptions, roughly 20% on average, is observed in the layer 200 to 50 hPa. The corresponding median values are 67.2 DU and 36.7 DU for the layers 100 to 50 hPa and 200 to 100 hPa for undisturbed years and 55 DU and 26 DU, respectively, after volcanic eruptions.

Two possible consequences for further steps could arise, namely modified statistical relations for disturbed and undisturbed years, and difficulties in assessing high $\Delta\Omega$ values due to the skewed distribution function of the predictands. The latter issue will be discussed in some detail later on.

3. Statistical approach

The statistical approach applied is the approach of multiple linear regression. An essential condition for the choice of potential predictors was the easy availability of these predictors in data banks confining their range to basic meteorological parameters such as geopotential, layer thickness, temperature, wind direction and velocity, and so on. Ozone data of previous days and thus persistence were not used. Thus some loss in the quality of the results is anticipated. The training sample consisted of ozone sonde and aerological data at Lindenberg (52°13'N, 14°07'E) and Hohenpeissenberg (47°48'N, 11°01'E) representing Central European conditions from the years 1975 to 1994. Multiple linear regression is a very reduced version of the general statistical approach outlined by *Pokrovsky* and *Timofeyev* (1972) where the solution is a combination of information on spectral radiance measurements and a priori meteorological knowledge by means of autocorrelation and crosscorrelation matrixes. This method was used as a pure statistical approach, i.e. without any measurement information, by *Timofeyev et al.* (1974) and later by *Feister* and *Spänkuch* (1977) who obtained encouraging results in ozone profiling when additionally to the temperature and temperature-ozone correlation the total ozone amount Ω was used as input with a maximum gain between about 300 and 50 hPa.

4. Statistical relations and reduction of variance

The quality of statistical relations is characterized by the reduction of variance achieved

$$RV = 1 - \left(\frac{\sigma_{re}}{\sigma_{cl}}\right)^2, \tag{1}$$

where σ_{re} and σ_{cl} mean the standard deviation between measurement and statistical estimate, and the climatological standard deviation, respectively. An exact physical relation results in $RV = 1$ ($\sigma_{re} = 0$). $RV = 0$ ($\sigma_{re} = \sigma_{cl}$) means that the statistical method does not give any more information against climatology. The stronger the statistical relation is the stronger, the higher the RV is.

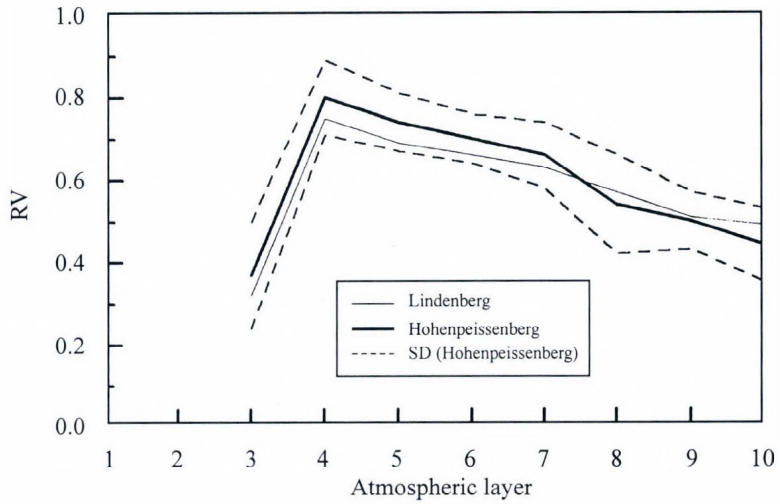

Fig. 2. Reduction of variance (*RV*) by statistical estimate of layer ozone.

Fig. 2 shows the yearly *RV* means at Lindenberg and Hohenpeissenberg, the latter one with $\pm$ the standard deviation of the monthly means. The altitude of the atmospheric layers increases with increasing number from p_s–700, 700–500, 500–300, 300–200, 200–150, 150–100, 100–70, 70–50, 50–30, and 30–20 hPa, respectively. The maximum values of *RV* are attained when all predictors of some significance even if marginal (e.g., $< 2\%$) are taken into account. The highest *RV* with about 0.8 is found for the tropopause region (layer 4: 300–200 hPa). There is a slow, steady decrease of *RV* within the stratosphere up to around 0.5 for layer 10 (30–20 hPa). Amounts larger than and around 0.7 are observed for the altitude range 300 to 100 hPa (layers 4 to 6) where monitoring from satellites is difficult and the height resolution of SBUV is limited. These results confirm previous investigations (e.g., *Spänkuch* and *Döhler*, 1975; *Fortuin* and *Kelder*, 1996) that stated maximum linear correlation between local ozone and temperature in the tropopause region and the lower stratosphere. *RV* is less than 0.3 in the troposphere. However, the climatological variance (σ_{cl}) is so small there (see Fig. 1) that the mean uncertainty of the

statistical estimate is only of the order of ± 1 Dobson units (DU) despite this low *RV*. The yearly course of *RV* at Hohenpeissenberg is given in *Fig. 3* for the atmospheric layers 300–200 hPa and 100–50 hPa, respectively. The highest *RV* is observed in general in winter and the smallest one in summer and fall.

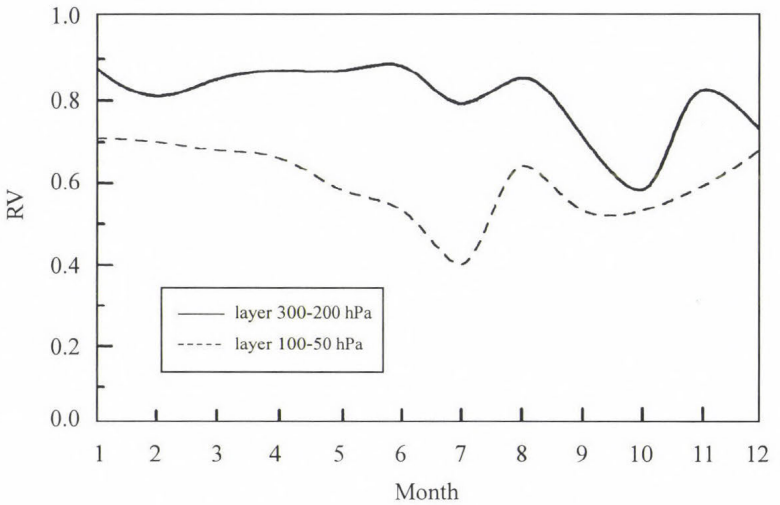

Fig. 3. Yearly course of *RV* for two atmospheric layers at Hohenpeissenberg.

Table 1 compiles the predictors and their contribution to *RV* for the four seasons for the multiple linear regression approach applied. The explanation of the predictors is given in the footnote of Table 1. The number of atmospheric layers was reduced, compared to the ones of Fig. 2, to safe space. Possible nonlinear dependence was taken into account to some extent by offering predictors with nonlinear dependence (e.g., logarithm or power) on basic meteorological parameters. There are six classes of predictors: column ozone Ω, temperature T_i at pressure levels i, layer thickness $\Delta\phi_i$, geopotential ϕ_i, normalized temperature gradient of layers $\nabla\check{T}_i$ and the saturation vapor pressure t_i or $\ln t_i$ as nonlinear parameters for the ith layer mean temperature. Although there is some redundancy by using layer thickness $\Delta\phi_i$ and saturation vapor pressure t_i as predictors simultaneously because both parameters are a function of the layer mean temperature t_m, the nonlinear dependence of t_i from t_m adds some useful information which is not appropriately taken into account by the linear dependence of $\Delta\phi$ from t_m. Table 1 contains two *RV* values, namely $RV_{max,\,total}$ when all predictors of significant even of marginal contributions were used, and RV_{total} when only predictors were used with a contribution to *RV* of

Table 1. Contribution of predictors in percentage to the reduction of variance of layer ozone for the four seasons

Layer	No	3				4				5				6				7			
	p (hPa)	300-200				200-100				100-50				50-30				30-10			
Predictor	Season	Sp	Su	Au	Wi	Sp	Su	Au	Wi	Sp	Su	Au	Wi	Sp	Su	Au	Wi	Sp	Su	Au	Wi
Ω		45	46	35	33	60	67	45	63	57	49	47	68	24	39	27		20	14	27	
ln Ω																	47				25
T_{500}							5													22	
T_{300}			7																		
T_{100}								11		13											
T_{50}						2															
T_{30}														6					9		
T_{10}																					4
$\Delta\phi_1$				14																	
$\Delta\phi_2$		8		17	13														5		
$\Delta\phi_3$			30	5	32																
$\Delta\phi_4$											4										
$\Delta\phi_5$															5	9	5				
$\Delta\phi_6$								17							4		5				
ϕ_4									6			13									
ϕ_6														5							
ln ϕ_7																					20
$\nabla\check{T}_5$							7														
$\nabla\check{T}_7$																		9		8	
t_3		30																			
t_5																					7
t_7																		23			
ln t_1											4										
RV, total		83	83	71	78	62	79	73	69	70	57	60	68	35	48	36	57	52	28	57	56
RV, max, total		86	87	73	82	72	83	77	79	75	69	64	75	48	57	41	63	56	32	64	60
Sum of predictors		3	3	4	3	2(7)	3	3	2	2	3	2	1	3	3	2	3	3	3	3	4

Explanation of the predictors: Ω – total column ozone in Dobson units, T_i – temperature (K) at pressure level i (hPa), ϕ_i and $\Delta\phi_i$ – geopotential and thickness in gpm of layer i, layers 1 and 2 are from surface pressure p_s to 500 hPa and from 500 to 300 hPa, respectively; $\nabla\check{T} = g_n \cdot (T_u - T_l) / T_l$ with T_u, T_l the temperatures at the upper and lower boundary, resp., of the layer given by the index, g_n – acceleration of gravity, t_i = saturation vapor pressure of layer i calculated from layer mean temperature.

at least 4 to 5 percent. The last line of Table 1 lists the number of predictors for RV_{total}. Three to four predictors are sufficient in general. RV_{total} can increase by about 0.1, e.g., for the layer 200 to 100 hPa in winter and spring, when 6 to 7 predictors instead of only 2 were considered.

The largest contribution to RV is from the total column ozone Ω or ln Ω, respectively, with a maximum reduction of about 2/3 for the layer 200–100 hPa (exception fall) and for the layer 100–50 hPa in winter, confirming the results of *Feister* and *Spänkuch* (1977). The RV_{total} is for the layer 200–100 hPa of the same order of magnitude in fall, too, due to the layer thickness of the sixth layer ($\Delta\phi_6$) and temperature at 100 hPa, T_{100}, as predictors.

Fig. 4 demonstrates the high correlation between Ω and layer ozone amount $\Delta\Omega$ for one single layer, the layer 200–150 hPa with a linear (upper panel) and a logarithmic regression approach (lower panel), the latter one is slightly more appropriate for large $\Delta\Omega$. The corresponding correlation coefficients are 0.80 and 0.78, respectively. The correlation was calculated with the Hohenpeissenberg data from 1975 to 1994. The single correlation coefficients between Ω and $\Delta\Omega$ are between 0.7 and 0.8 for 300 to 30 hPa, about 0.4 for 30 to 10 and 500 to 300 hPa and insignificant in the lower troposphere.

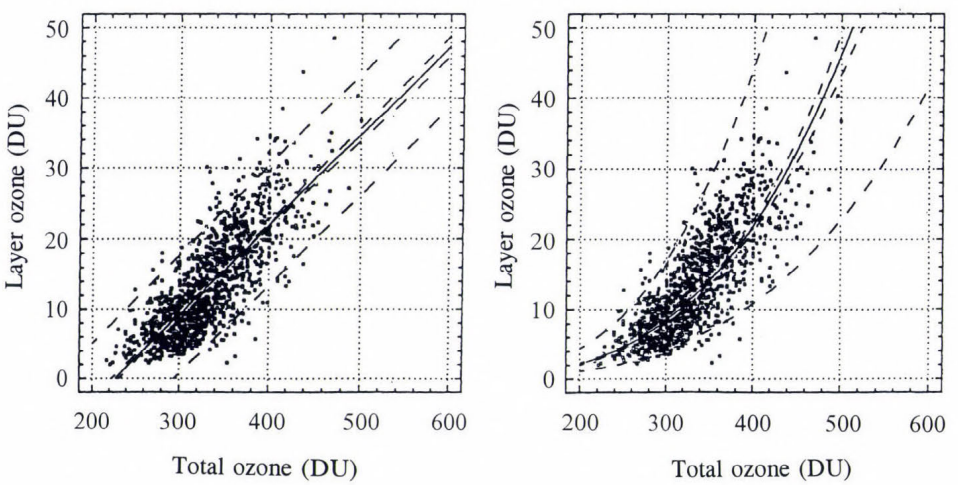

Fig. 4. The relation between layer ozone between 200 to 150 hPa and total ozone at Hohenpeissenberg.

Layer thicknesses ($\Delta\phi$) of the lower layers contribute significantly to RV in the tropopause region (300 to 200 hPa), except for spring. Their total contribution is about 0.4 and of the same order of magnitude as the contribution of Ω.

In spring, the saturation vapor pressure of layer 3, t_3, of the tropopause layer contributes 30% to *RV*. This order of magnitude is only reached for the layer 30 to 10 hPa in spring by the analogous parameter t_7. For this layer *RV* is about 0.5 and even only 0.3 in summer with half of the contribution from Ω. The high contribution of predictors characterizing the thermal state of the tropopause region is mainly due to quasi-columnar motion of air along isentropic surfaces in the lower stratosphere which explaines more than half of the variance of Ω (*Salby* and *Callaghan*, 1993).

The effect of the individual predictors is illustrated by a single example, and that for the tropopause region 300 to 200 hPa in May over Hohenpeissenberg. The maximum RV considering 6 predictors is 0.87 (see Table 1). Using as single predictors only the most effective ones, Ω and T_{200}, respectively, results in *RV* amounts of 0.55 and 0.69, respectively (*Fig. 5* upper panels). Obviously, T_{200} is a more appropriate predictor than Ω in this case. Fig. 5 shows that both single regression equations estimate ΔΩ up to 30 DU in maximum only, in contrast to the observation with 44 DU in maximum. There is an increase of *RV* to 0.75 using both predictors simultaneously (Fig. 5, lower left panel), however, the deficit remains at high ΔΩ. A sufficient estimate of ΔΩ for high ΔΩ is only reached when further predictors are added (Fig. 5, lower right panel). Note that in case of more predictors T_{200} is replaced by T_{300} (see Table 1).

5. Impact of predictor uncertainty on the quality of the statistical estimate

Another feature of interest besides the individual predictors' contribution to *RV* is the sensitivity of the quality of the statistical estimate to the quality of the predictors. This information is easily derived from the magnitude of the regression coefficients and compiled in *Table 2*. The numbers of Table 2 are related to a change in the estimate of ΔΩ in the corresponding atmospheric layer by 1 DU caused by a change of the specific predictor by the amount given. The figures of Table 2 are related to DU and K for Ω, ln Ω and T_i, respectively, and in per cent of the natural variation of the rest of the predictors. The estimate of ΔΩ is most sensitive to the temperature if this predictor is used. A change, e.g., of the ΔΩ estimate of the layer 100 to 50 hPa in spring by +1 DU is caused by a change of T_{100} by –0.5 K. This uncertainty of about 1 K results in a 2 DU uncertainty of the ΔΩ assessment already. A similar magnitude (–0.7 K) was found for T_{300} in assessing ΔΩ in the tropopause region in summer as well as for T_{100} for the 200 to 100 hPa layer in fall. The temperature uncertainty is less crucial for the other cases with temperature as a predictor.

Uncertainties in Ω are most effective for the ΔΩ assessment in that layers with a high contribution of Ω to *RV*, namely for the layers 200 to 100 hPa and 100 to 50 hPa. A 1 DU change in ΔΩ there corresponds to 3 to 5 DU in the uncertainty of Ω. However, the rule "high contribution to *RV* of a predictor

corresponds to high sensitivity to the statistical $\Delta\Omega$ estimate" does not hold unconditionally as shown by a comparison of the corresponding amounts for the layers 300 to 200 hPa and 50 to 30 hPa, respectively.

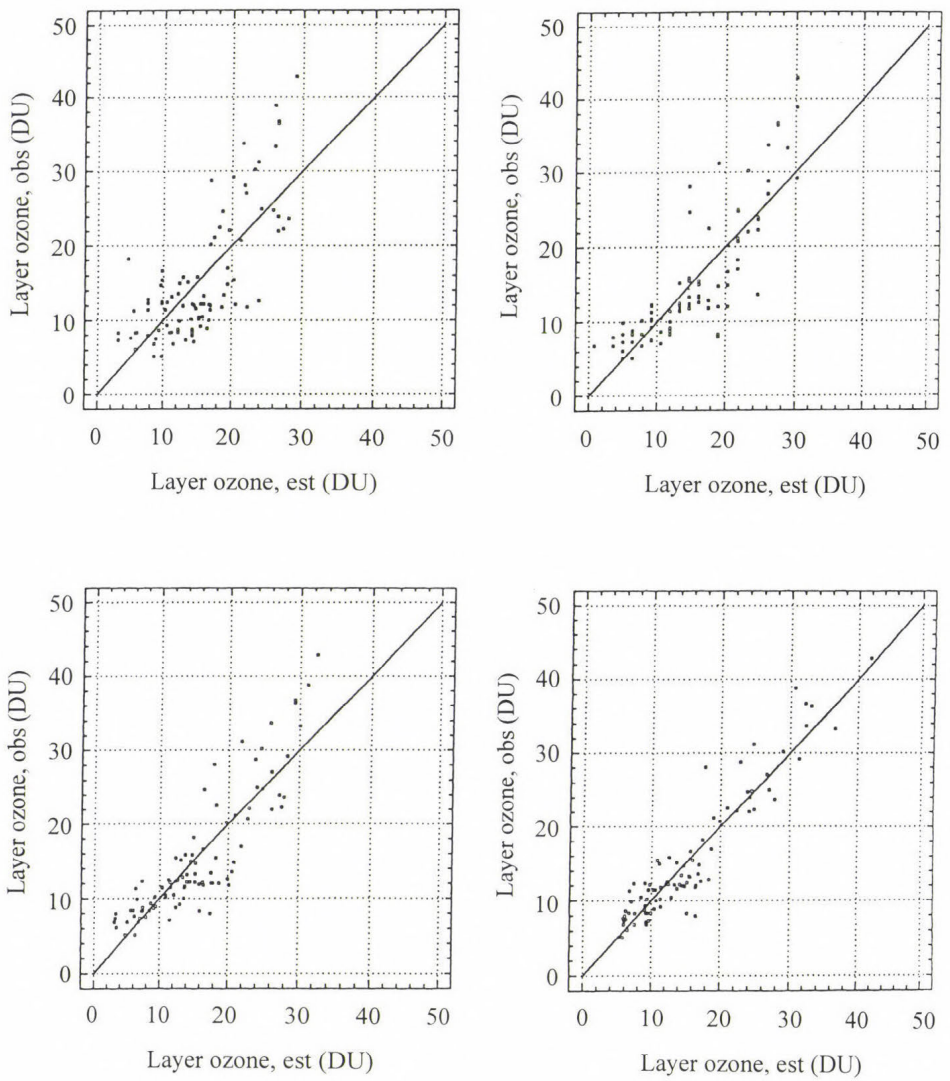

Fig. 5. Comparison of observed and estimated layer ozone in the tropopause region 300–200 hPa at Hohenpeissenberg in May with predictors Ω only (upper left panel), T_{200} only (upper right panel), Ω plus T_{200} (lower left panel) and all significant six predictors (lower right panel).

Table 2. Predictors' order of magnitude to change layer ozone estimate by 1 DU

Layer	No	3				4				5				6				7			
Predictor	p (hPa) Season	300-200 Sp	Su	Au	Wi	200-100 Sp	Su	Au	Wi	100-50 Sp	Su	Au	Wi	50-30 Sp	Su	Au	Wi	30-10 Sp	Su	Au	Wi
Ω		18	17	27	35	3	5	4	4	3	5	5	3	13	9	6		20	8	4	
ln Ω																	9				10
T_{500}							1.6													1	
T_{300}			.7																		
T_{100}								.7		.5											
T_{50}						2															
T_{30}														5					1.3		
T_{10}																					3
$\Delta\phi_1$				25																	
$\Delta\phi_2$		5		6	5														8		
$\Delta\phi_3$			4	8	6																
$\Delta\phi_4$											7										
$\Delta\phi_5$															8	9	5				
$\Delta\phi_6$								3							5		5				
ϕ_4									3			6									
ϕ_6														12							
ln ϕ_7																					7
∇T_5							8														
∇T_7																		4		3.5	
t_3		2																			
t_5																					5
t_7																		2.5			
ln t_i											80										

Explanation of the predictors see Table 1. The figures for all parameters except Ω, ln Ω and T_i are the percentage of natural variability of the corresponding parameter. For Ω and ln Ω the figures are in DU, for T_i in K.

Satellite measurements of Ω are estimated to be accurate to $\pm 2\%$ or ± 8 DU (*Fleig et al.*, 1990; *Herman et al.*, 1991), and Ω forecasting is claimed to be accurate to ± 3 to 4% or ± 10 to 12 DU (*Burrows et al.*, 1995; *Spänkuch* and *Schulz*, 1995, 1997a; *Long et al.*, 1996). The resulting uncertainty in assessing $\Delta\Omega$ for the altitude range from 200 to 50 hPa is ± 2 DU when satellite measurements will be used, and ± 3 to 4 DU in case of predicted Ω. For all other predictors a change in the estimate of $\Delta\Omega$ by 1 DU is caused by a change of the predictors by about 5 to 10 per cent of the predictors' natural variability, which is equal to the order of magnitude of the measurement and analysis error.

The resulting inaccuracy in the $\Delta\Omega$ estimate due to measurement and/or analysis errors is assessed to be about 3 to 4 DU when Ω is taken from satellite measurements. Consequently, the attainable maximum accuracy of $\Delta\Omega$ is about 3 to 10 per cent for the individual atmospheric layers (see Fig. 1).

6. Results

The results of layer ozone estimates at Hohenpeissenberg during the year 1996 as independent sample with more than 100 individual cases are shown in the scatter plots of *Fig. 6* and summarized in *Table 3*. Given are the results for each layer for completeness, even in case of only marginal improvement against climatology as for the tropospheric layers, and in total for the layer 300 to 50 hPa, where the most significant improvement was found. Fig. 6 reveals several interesting aspects. First, we note a negative bias of the $\Delta\Omega$ estimate ($\Delta\Omega_{est} < \Delta\Omega_{meas}$) of about 1 to 2 DU up to 50 hPa (see Table 3) and a positive bias above that level. In August 1995, the radiosonde type was changed from VIZ 1993 of VIZ Manufacturing, Philadelphia, USA, to RS 80 of Vaisala, Finland. Both radiosondes use different devices for pressure measurements resulting not only in differences in the pressure values measured (*Nash* and *Schmidlin* (1987) and *Ivanov et al.* (1991) for details), but also in differences in temperature and ozone. The resulting differences in ozone are up to 6 per cent above 26 km (20 hPa) and, due to the impact on the Dobson correction, up to about 1.5 per cent below 20 km (50 hPa) (*Steinbrecht* 1998, private communication). Thus the bias is not real and only the impact of the inhomogeneity in the Hohenpeissenberg data. The corresponding *rms* of the estimate without this virtual bias is given in brackets in Table 3.

Second, there is a rate of about 8 to 10 per cent outliers with considerable underestimation in $\Delta\Omega$ for high $\Delta\Omega$ amounts in the layers below 100 hPa particularly distinct in the layer 200 to 100 hPa, with unacceptable large errors

Fig. 6. Comparison of observed and estimated layer ozone at Hohenpeissenberg in 1996 (independent sample). Note the different scales of the panels.☞

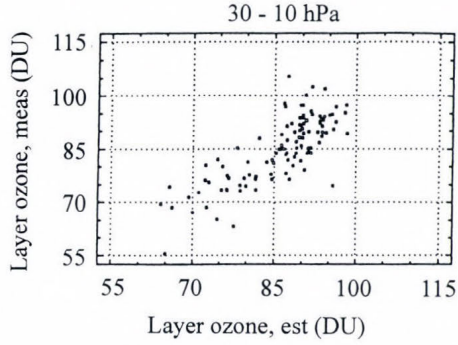
30 - 10 hPa
Layer ozone, meas (DU)
115
100
85
70
55
55
70
85
100
115
Layer ozone, est (DU)

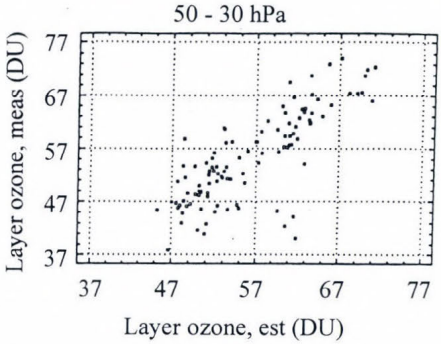
50 - 30 hPa
Layer ozone, meas (DU)
77
67
57
47
37
37
47
57
67
77
Layer ozone, est (DU)

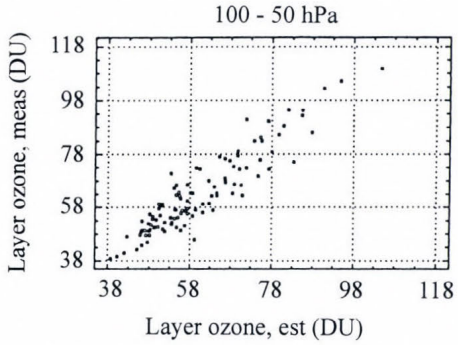
100 - 50 hPa
Layer ozone, meas (DU)
118
98
78
58
38
38
58
78
98
118
Layer ozone, est (DU)

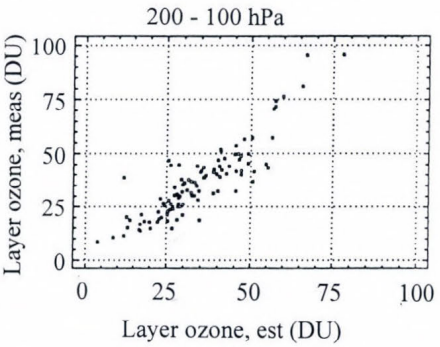
200 - 100 hPa
Layer ozone, meas (DU)
100
75
50
25
0
0
25
50
75
100
Layer ozone, est (DU)

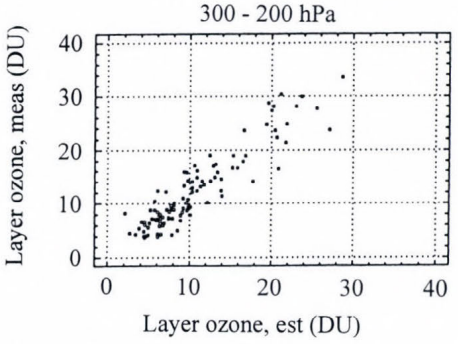
300 - 200 hPa
Layer ozone, meas (DU)
40
30
20
10
0
0
10
20
30
40
Layer ozone, est (DU)

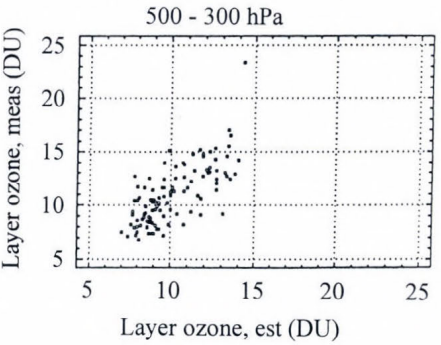
500 - 300 hPa
Layer ozone, meas (DU)
25
20
15
10
5
5
10
15
20
25
Layer ozone, est (DU)

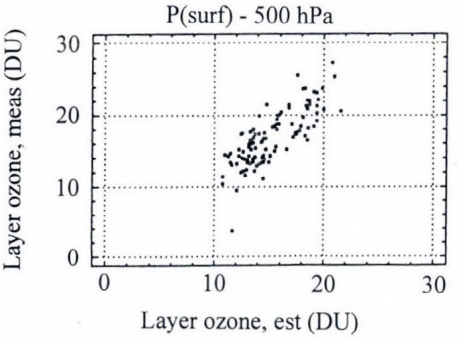
P(surf) - 500 hPa
Layer ozone, meas (DU)
30
20
10
0
0
10
20
30
Layer ozone, est (DU)

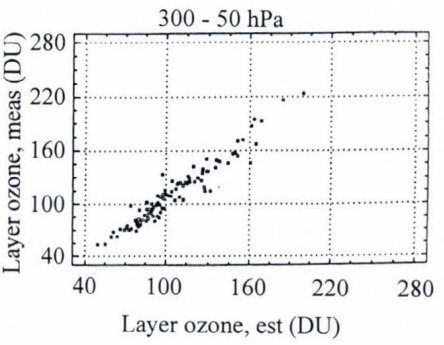
300 - 50 hPa
Layer ozone, meas (DU)
280
220
160
100
40
40
100
160
220
280
Layer ozone, est (DU)

of 15 DU and more. In all these cases filament-like structures were found. Thus the results of the approach have to be taken with care in such cases that can be characterized by a $\Delta\Omega$ estimate larger than a certain threshold to be defined by further studies. The present results suggest, e.g., about 58 DU as threshold for the layer ozone between 200 and 100 hPa, and about 160 DU for the layer 300 to 50 hPa. In the latter case the bias is about –20 DU. *Appenzeller* and *Holton* (1997) investigating the climatology of filament-like structures in the stratosphere, found three geographic areas of favourable occurrence of filaments, all linked to the edge of the polar vortex, namely Europe, Siberia and Northern Canada.

Table 3. Results of layer ozone estimate 1996

Layer (hPa)	Bias (DU)	σ_{cl}	σ_{es} (DU)	rms (DU)	r^2	Change (%)
p_s –500	–1.5	3.8	2.4	2.8 (2.2)	0.53	64
500–300	–0.8	2.8	1.9	2.1 (1.7)	0.55	63
300–200	–1.6	7.0	2.8	3.2 (2.6)	0.85	83
200–100	–1.8	16.6	7.9	8.1 (7.2)	0.77	80
100 – 50	–2.6	14.8	5.8	6.3 (5.5)	0.85	67
50 – 30	1.2	8.4	5.2	5.4 (4.7)	0.59	56
30 – 10	1.2	9.3	5.9	6.0 (5.4)	0.62	70

The most satisfying results were achieved for the layers 300 to 200 hPa and 100 to 50 hPa with the square of the linear regression coefficient of 0.85 in both cases (Table 3). Omitting the outliers which are mostly found in the $\Delta\Omega$ estimate of single layers, we state satisfying results for the lower stratosphere up to 50 hPa, as demonstrated in the corresponding panels of Fig. 6.

The statistical estimate of $\Delta\Omega$ for the troposphere in particular, and above 50 hPa is to be taken only as a kind of first guess as expected from the discussion of Chapter 3. Nevertheless, the estimate of the sign of the diurnal changes in $\Delta\Omega$ given in the last column of Table 3 is with 70 per cent for the layer 30 to 10 hPa like the one of the layer 100 to 50 hPa. Again, the highest rate with 83 per cent in the correct estimate of the sign of the diurnal change is found for the layer 300 to 200 hPa.

7. Summary and conclusions

A multiple linear regression approach is presented to estimate layer ozone amount $\Delta\Omega$ from predictors accessible from model outputs of meteorological analysis and prediction additionally to the total ozone amount that has regularly been monitored from satellites for several years. Total column ozone is the most important predictor in general of the approach developed and checked for northern midlatidudes. The second most important predictor is the thermal state of atmospheric layers. The accuracy of the statistical estimate is assessed to be about 3 to 10 per cent in maximum dependent on atmospheric layer and season. Comparison of the estimate with more than one hundred ozone sonde data at Hohenpeissenberg, Germany, throughout one year showed promising results between 300 and 50 hPa when outliers of about 8 to 10 per cent of cases are omitted. The outliers were mainly found for the layer between 200 and 100 hPa and are obviously related to filament-like structures in ozone there. The most satisfying results were obtained for the tropopause region 300–200 hPa with a reduction of variance of about 0.7 to 0.8.

Acknowledgement—The authors are pleased to acknowledge support of this research by the Bundesministerium für Forschung und Technologie (BMFT) through Grant No. 01 L0 9509 9.

References

Appenzeller, C. and *Holton, J.R.*, 1997: Tracer lamination in the stratosphere: A global climatology. *J. Geophys. Res. 102,* 13,555-13,569.

Burrows, W.R., Vallée, M., Kerr, J.B., Wilson, L.J. and *Tarasick, D.W.*, 1995: The Canadian operational procedure for forecasting total ozone and UV radiation. *Meteorol. Appl. 1*, 247-265.

Dütsch, H.U., 1978: Vertical ozone distribution on a global scale. *Pure Appl. Geophys. 116*, 511-529.

Fabian, P., 1989: *Atmosphäre und Umwelt.* Springer Verlag, Berlin.

Feister, U. and *Spänkuch, D.*, 1977: The deviation of the vertical ozone profile from statistical relations. In *Proc. Joint Symposium on Atmospheric Ozone*, Vol. I., (ed.: *K.H. Grasnick*). Dresden, 9-17 August 1976. 331-360, Berlin.

Fleig, A.J, Mc. Peters, R.D., Bhartia, P.K., Schlesinger, B.M., Cebula, R.P., Klenk, K.F., Taylor, S.L. and *Heath, D.F.*, 1990: Nimbus 7 solar backscatter ultraviolett (SBUV) ozone products user's guide. *NASA Ref. Publ.*, 19-25.

Fortuin, J.P.F. and *Kelder, H.*, 1996: Possible links between ozone and temperature profiles. *Geophys. Res. Lett. 23*, 1517-1520.

Götz, F.W.P., 1931: Zum Strahlungsklima des Spitzbergensommers. *Gerlands Beitr. Geophys. 95*, 119-154.

Herman, J.R., Hudson, R., Mc. Peters, R.D., Stolarski, R., Gu, X.-Y., Taylor, S. and *Wellenmeyer, C.*, 1991: A new self-calibration method applied to TOMS and SBUV backscattered ultraviolet data determine long-term global ozone change. *J. Geophys. Res. 96*, 7531-7545.

Ivanov, A., Kats, A., Kurnosenko, S., Nash, N. and *Zaitseva, N.*, 1991: WMO International Radiosonde Comparison. Phase III, (Dzhambul, USSR, 1989). World Meteorological Organization, Instruments and Observing Methods. *Report 40, WMO/TD-NO. 451*, Genf.

Krzyścin, J.W., 1994: Total ozone changes in the northern hemisphere mid-latitudinal belt (30–60°N) derived from Dobson Spectrophotometer measurements, 1964–1988. *J. Atmos. Terr. Phys. 56*, 1051-1056.

Lacis, A.A., Wuebbles, D.J. and *Logan, J.A.*, 1990: Radiative forcing of climate by changes in the vertical distribution of ozone. *J. Geophys. Res. 95*, 9971-9981.

Long, C.S., Miller, A.J., Lee, H.-T., Wild, J.D., Przywarty, R.C. and *Hufford, D.*, 1996: Ultraviolet index forecast issued by the National Weather Service. *Bull. Amer. Meteorol. Soc. 77*, 729-748.

de Luisi, J.J. and *Mateer, C.L.*, 1971: On the application of the optimum statistical inversion technique to the evaluation of Umkehr observations. *J. Appl. Meteorol. 10*, 328-334.

Nash, J. and *Schmidlin, F.J.*,1987: WMO International Radiosonde Comparison (U. K. 1984, USA 1985). World Meteorological Organization, Instruments and Observing Methods. *Report 30, WMO/TD-NO. 195*, Genf.

Pokrovsky, O.M. and *Timofeyev, Yu.M.*, 1972: A general statistical approach for the solution of inverse problems of atmospheric optics (in Russian). *Meteorol. Gidrol. No. 1*, 52-59.

Ramaswamy, V., Schwarzkopf, M.D. and *Shine, K.P.*, 1992: Radiative forcing of climate from halocarbon-induced global stratospheric ozone loss. *Nature 355*, 810-812.

Roan, S.L., 1989: *Ozone Crisis: The 15-year Evolution of a Sudden Global Emergency*. Wiley, New York.

Salby, M.L. and *Callaghan, P.F.*, 1993: Fluctuations of total ozone and their relationship to stratospheric air motions. *J. Geophys. Res. 98*, 2715-2727.

Seliers, W.D. and *Yarger, D.N.*, 1969: The statistical prediction of the vertical ozone distribution. *J. Appl. Meteorol. 8*, 357-361.

Spänkuch, D. and *Döhler, W.*, 1975: Statistische Characteristika der Vertikalprofile von Temperatur und Ozon und ihre Korrelation über Berlin. *Geodät. und Geophys. Veröff., Reihe II, Heft 19*.

Spänkuch, D. and *Schulz, E.*, 1995: Diagnosing and forecasting total column ozone by statistical relations. *J. Geophys. Res. 100*, 18,873-18,885.

Spänkuch, D. and *Schulz, E.*, 1997a: On short-term total-column-ozone-forecast errors. *Atmos. Environment 31*, 117-120.

Spänkuch, D. and *Schulz, E.*, 1997b: Quality checks for satellite and ground-based total ozone observations. In *Ground-level and Satellite Observations: Changes in the Mediterranean Region* (ed.: *C. Varotsos*). Springer-Verlag, Berlin-Heidelberg, 293-302.

Timofeyev, Yu.M., Kucnecov, A.D. and *Spänkuch, D.*, 1974: About the retrieval accuracy of the atmospheric ozone profile. In *Radiative Processes in the Atmosphere and at the Surface* (in Russian). Trudy Allunions-Meeting on Actinometry. Nauka, Kiev, 126-130.

WMO, 1995: *Scientific Assessment of Ozone Depletion: 1994, 1995: World Meteorological Organization Global Ozone Research and Monitoring Project-Report No. 37, Geneva.*

IDŐJÁRÁS

Quarterly Journal of the Hungarian Meteorological Service
Vol. 102, No. 4, October–December 1998, pp. 219–237

Characterizing air pollution potential over Budapest using macrocirculation types

I. Matyasovszky and **T. Weidinger**

Department of Meteorology, Eötvös Loránd University,
H-1117 Budapest, Pázmány Péter sétány 1, Hungary; E-mail: matya@ludens.elte.hu

(Manuscript received 23 February 1998; in final form 15 June 1998)

Abstract—Time series of height of planetary boundary layer (PBL), mean virtual temperature gradient of the lower 300 m, wind speed at 925 hPa pressure level and energy of instability (in the lower 1 km in winter and lower 2 km layer in summer) were calculated using radiosonde data (1962–1992) over Budapest. These parameters principally determine the air pollution potential, i.e., the capacity of mixing of pollutants. Using daily radiosonde data (12 UTC), parameters characterizing air pollution potential are related to Hess-Brezowsky (HB) macrocirculation (MC) types in winter and summer seasons. However, the large number of HB types (30 HB types) makes it difficult to evaluate the statistical relationship, therefore, an algorithm is developed to define a family of MC types obtained by aggregating the HB types. A similarity measure of MC types is defined and used on a seasonal basis in terms of PBL parameters. The family of MC types consisting of 16, 12, 8 and 4 types are shown. For 8 types, a multivariate time series model of PBL parameters is developed and checked. The model is able to simulate statistical properties of PBL parameters under present conditions and then under different hypothetical conditions.

Key-words: air pollution potential, planetary boundary layer, macrocirculation types.

1. Introduction

The capacity of the atmosphere to disperse and dilute pollutants emitted at different scale sources depends upon prevailing meteorological conditions of planetary boundary layer (PBL), such as the height, temperature gradient (stability), wind direction and wind speed, wind shear, and energy of instability of the PBL (*Szepesi et al.*, 1977). These parameters characterize air pollution potential of a given area. The term air pollution potential has been introduced in the seventies and characterizes the ability of loading of the atmosphere by pollutants (*Wiswanadham* and *Santosh*, 1989). The statistical relationship between the macrocirculation types and air pollution potential is an important

issue in order to know how the air pollution characteristics relate to the actual weather. This problem is crucial in case of extreme pollution situations. There is a general empirical knowledge of which weather situations are problematic in the presence of pollutants in the atmosphere, but the present paper is directed at developing a stochastic model to describe this relationship quantitatively.

The ultimate purpose of our work is to develop a multivariate time series model in order to simulate statistical properties of PBL parameters under present conditions and then under different hypothetical conditions of large-scale atmospheric circulation. It is well-known that behavior of meteorological parameters strongly depend on macrocirculation. Therefore, a system of macrocirculation (MC) types is used as a relevant additional information, namely the time series model is related to MC types. The paper reports the present stage of our research.

The first step of developing the model is estimating the probability distribution of PBL parameters controlling air pollution potential. This step was performed by conditioning probability distributions on Hess-Brezowsky (HB) macrocirculation types using radiosonde data for Budapest. However, the large number of HB types (30 HB types) makes it difficult to evaluate the statistical relationship, therefore, an algorithm is developed to define a family of MC types obtained by aggregating the HB types. A similarity measure of MC types is defined and used on a seasonal basis in terms of PBL parameters. Then, a multivariate time series model is developed and is presented under 8 MC types.

First, data sets used in the analysis are presented and dependency of statistical behavior of PBL parameters on HB types is demonstrated. Next, the methodology and results of aggregating HB types resulting in a new system of MC types are reported. Then, properties of time series model reproducing observed statistics are discussed. Finally, a section for conclusions is provided.

2. Characterizing data

Archived and checked radiosonde data for Budapest are available for several years. A data set from 1962 to 1992 is used for analyzing PBL parameters. Winter (December, January, February) and summer (June, July, August) seasons are considered separately with 12 UTC observations. Four parameters have been defined to characterize PBL:

- height of PBL (H [m]),
- gradient of virtual potential temperature in the lower 300 m (γ_V [°C/100 m]),
- wind speed at the 925 hPa standard pressure level (V [m/s]),
- energy of instability (A [J/kg]) in the lower 1 km layer in winter and in the lower 2 km layer in summer in accordance with yearly course of convective PBL height.

A first overall theoretical study of PBL in Hungary was reported by *Bodolai* (1983). Here, the height of PBL is determined by significant points of virtual temperature profile. No unique definition exists for determining the height of convective PBL (*Stull*, 1988). We defined the top of the PBL at the highest significant point where the mean virtual temperature gradient between the surface and that significant point is larger than or equal to 0.95°C/100 m and the virtual temperature gradient below this significant point is larger than or equal to 0.8°C/100 m (the larger this threshold the smaller the estimated PBL height is). We used the so-called modified bubble method for dry adiabatic condition. Sensitivity analysis shows an uncertainty of 10–15 % (*Weidinger et al.*, 1996).

The energy of instability is calculated as:

$$A = \int_{z_0}^{z_1} g \frac{T_v^* - T_v}{T_v} dz, \tag{1}$$

where z_0 and z_1 denotes the lower and upper height of the layer for calculation energy of instability, g is the acceleration due to gravity, T_v and T_v^* correspond to the virtual temperature of environment and the rising air parcel from surface (z_0) by pseudo-adiabatic process.

The usefulness of these parameters is demonstrated by *Table 1*. Statistically significant relations can be identified between virtual temperature gradient and energy of instability, as well as between energy of instability and the height of PBL. In the rest of cases correlation values are quite low (but different from zero at a 5 % significance level due to large sample sizes) indicating that each variable has a large amount of information not contained in other variables.

Table 1. The mean (m), standard deviation (σ) and correlation matrix of PBL characteristics

	Winter						Summer					
	m	σ	Correlation matrix				m	σ	Correlation matrix			
H	604	380	1.00	0.30	0.03	0.53	1406	603	1.00	0.17	-0.10	0.30
γ_v	0.69	0.50	0.30	1.00	-0.09	0.76	1.15	0.27	0.17	1.00	-0.08	0.64
V	8.1	4.8	0.03	-0.09	1.00	-0.03	5.4	3.3	-0.10	-0.08	1.00	-0.14
A	-66.5	69.7	0.53	0.76	-0.03	1.00	39.9	69.1	0.30	0.64	-0.14	1.00

H – height of PBL, γ_v – gradient of potential temperature in the lower 300 m, V – wind speed at the 925 hPa standard pressure level, A – energy of instability (in the lower 1 km in winter and in the lower 2 km in summer)

Hess-Brezowsky macrocirculation types are well-known in meteorological literature; their basic properties are summarized in *Table 2* (*Hess* and *Brezowsky*, 1969; *Bartholy* and *Kaba*, 1987). In order to demonstrate the dependency of PBL parameters on HB types some results for probability distribution of parameters characterizing air pollution potential are shown next for winter and summer under two characteristic HB types. NWz (Northwest cyclonic) type usually advects oceanic air masses. NWz produces mostly positive temperature anomalies (–1 – +3°C) in winter, while causes negative anomalies (–1 – –3°C) in summer. The relative frequency of this type is 6.4% in winter and 4.9% in summer. HM (Central European high) type is characterized mostly with continental air masses resulting in negative temperature anomalies (–2.5 – –1.5°C) in winter and positive anomalies (0.5–1.0°C) in summer. Relative frequency of this type is 7.4% in winter and 6% in summer.

Table 2. Definition of HB types

Major types	Subtypes		Subtypes	
		Zonal		
West	1. West anticyclonic	Wa	2. West cyclonic	Wz
	3. Southern West	Ws	4. Angleformed West	Ww
		Half-meridional		
Southwest	5. Southwest anticyclonic	SWa	6. Southwest cyclonic	SWz
Northwest	7. Northwest anticyclonic	NWa	8. Northwest cyclonic	NWz
Central European high	9. Central European high	HM	10. Central European ridge	BM
Central European low	11. Central European low	TM		
		Meridional		
North	12. North anticyclonic	Na	13. North cyclonic	Nz
	14. North, Iceland high, anticyclonic	HNa	15. North, Iceland high, cyclonic	HNz
	16. British Islands high	HB	17. Central European trough	TrM
Northeast	18. Northeast anticyclonic	NEa	19. Northeast cyclonic	NEz
East	20. Fenno-scandinavian high anticyclonic	HFa	21. Fenno-scandinavian high cyclonic	HFz
	22. Norwegian Sea-Fenno-scandinavian high anticyclonic	HNFa	23. Norwegian Sea-Fenno-scandinavian high cyclonic	HNFz
Southeast	24. Southeast anticyclonic	SEa	25. Southeast cyclonic	SEz
South	26. South anticyclonic	Sa	27. South cyclonic	Sz
	28. British Islands low	TB	29. Western Europe trough	TrW
	30. Unclassified	Ü		

Depending on types, the mean PBL height is around 500–800 m in winter, and is 1250–1650 m in summer. The Weibull distribution fits the histograms best for both seasons and both types. The hypothesis that PBL height follows Weibull distributions in these types can be accepted at least at a 5% significance level. However, when using the entire data set the best fitting distribution is lognormal in winter (*Fig. 1*).

The gradient of potential temperature in the lower 300 m ($\gamma_v = -\Delta T_v / \Delta z$, $\Delta z = 300$ m) cannot be satisfactorily modeled by any well-known probability distribution (*Fig. 2*). In winter, the mean gradient is somewhat larger for NWz (0.74°C/100 m) than for HM (0.67°C/100 m). The instability intensifies in summer: the difference between the HB types is considerably smaller (1.2–1.05°C/100 m) than in winter (0.99–0.5°C/100 m). The HM type produces stronger instability than the cyclonic NWz type.

Flows of PBL are described by speed and direction of wind at the 925 hPa standard pressure level (*Fig. 3*). Wind roses of the HM type are similar and characterized by frequent northwestern, northern, northeastern directions in both seasons, while the relative frequency of northwestern direction exceeds 40% in NWz type. The mean wind speed in winter is between 5.6 m/s and 11.5 m/s depending on types. The summer exhibits a considerably smaller difference between mean wind speeds in each HB type. The entire set of winter wind speeds is best fitted by a Weibull distribution, while the most suitable distribution is the lognormal in summer. In winter, NWz and HM types can be described by a normal and a lognormal distribution, respectively. Both types require a Weibull distribution in summer. Statistical tests (chi-square and Kolmogorov-Smirnov tests) show that the distributions fit the data substantially better for NWz type than in the case of HM accompanied with smaller wind speeds. The wind turning between 925 hPa standard pressure level and the surface has a remarkable property (*Fig. 4*). Namely, the wind turns left (reverse from Ekman spiral) with the height with relative frequencies of 25% in winter and 50% in summer.

Energy of instability was calculated for different layers in winter and summer due to the annual cycle of the convective PBL height. The mean energy of instability is obviously negative in winter and positive in summer for each HM type. The absolute value of mean energy of instability naturally was higher in the HM anticyclonic type than in the NWz cyclonic type in both seasons (*Fig. 5*). Commonly used distribution functions cannot fit the histograms in the majority of types.

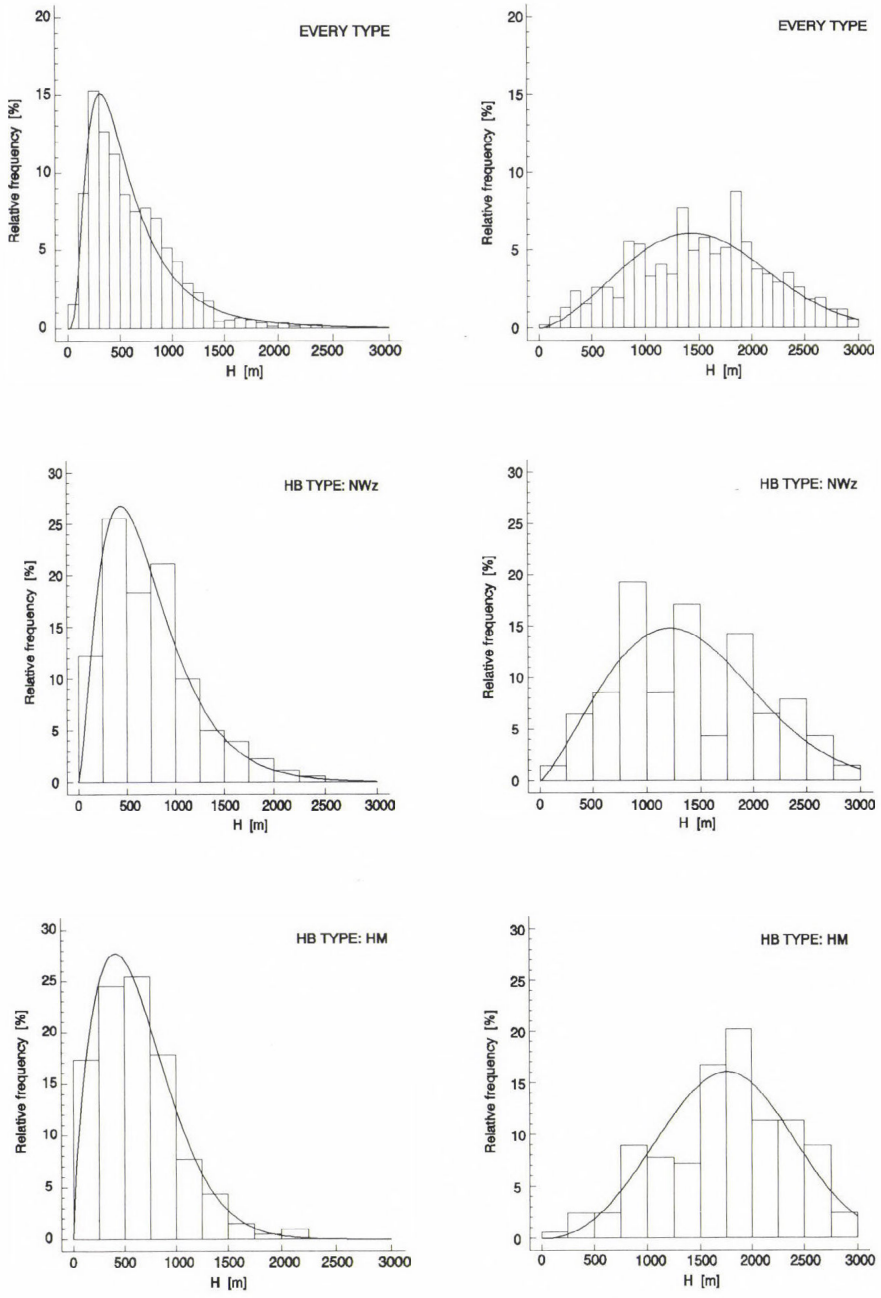

Fig. 1. Probability density of height of PBL in winter (left) and summer (right).

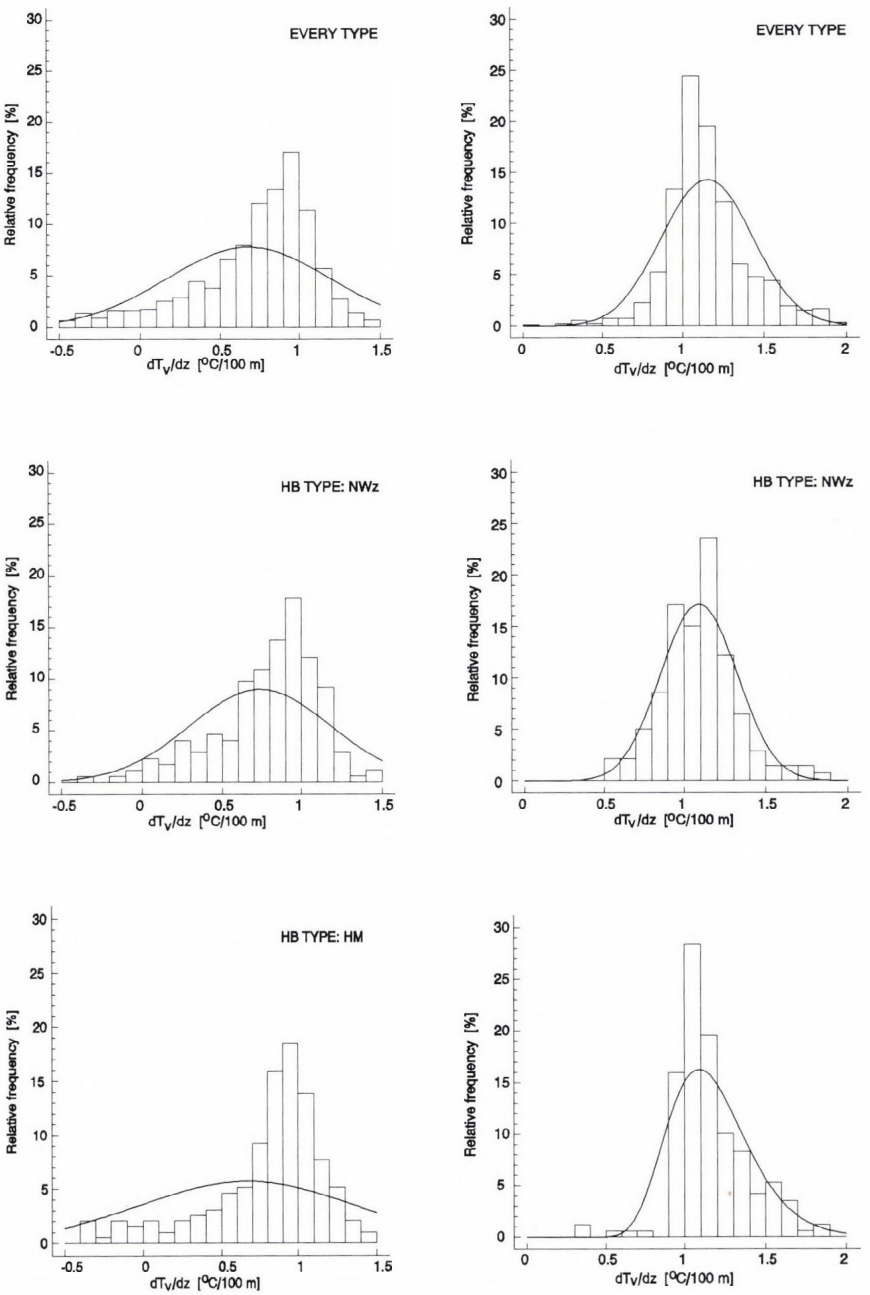

Fig. 2. Probability density of gradient of virtual temperature [°C/100 m] in the lower 300 m in winter (left) and summer (right).

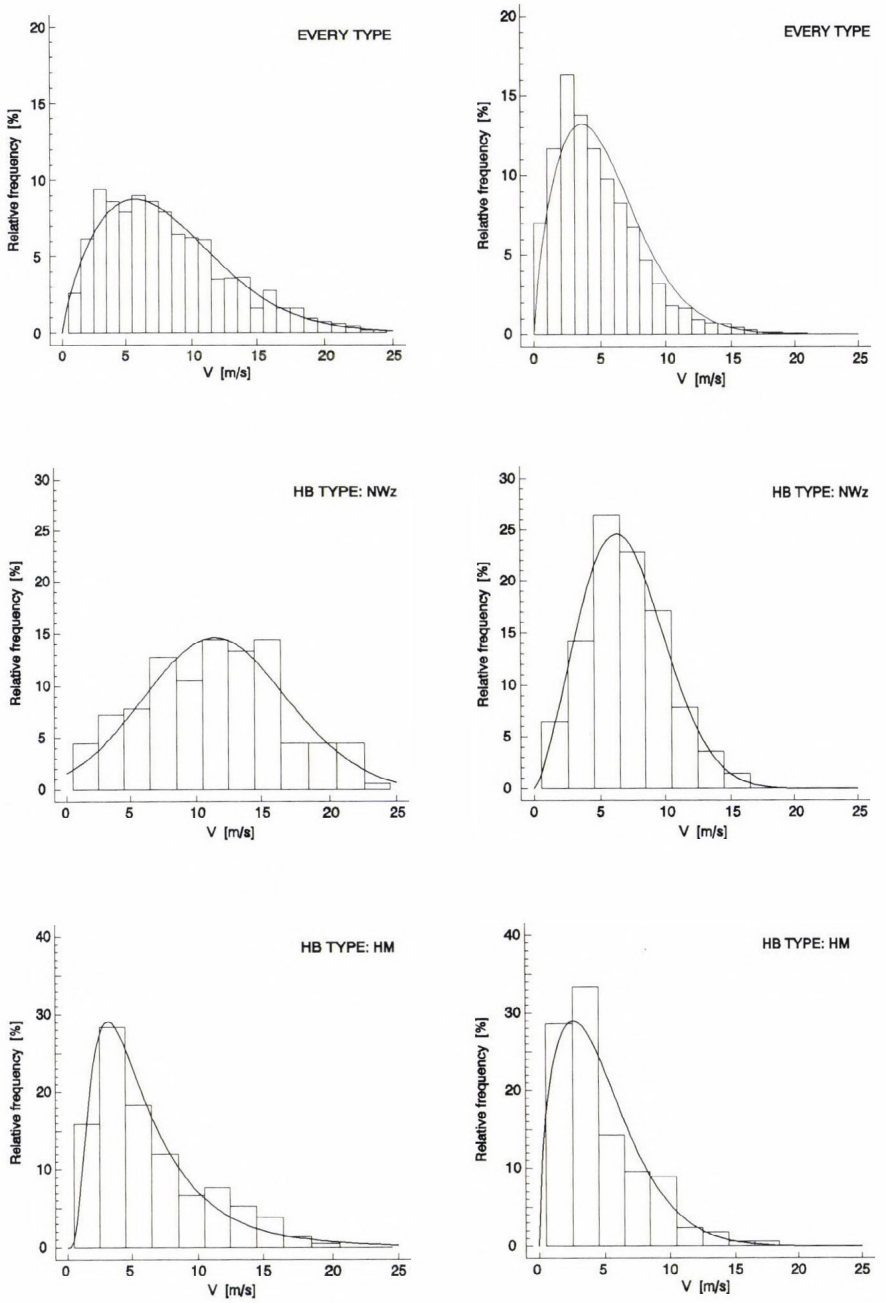

Fig. 3. Probability density of speed and direction of wind at the 925 hPa standard pressure level in winter (left) and summer (right).

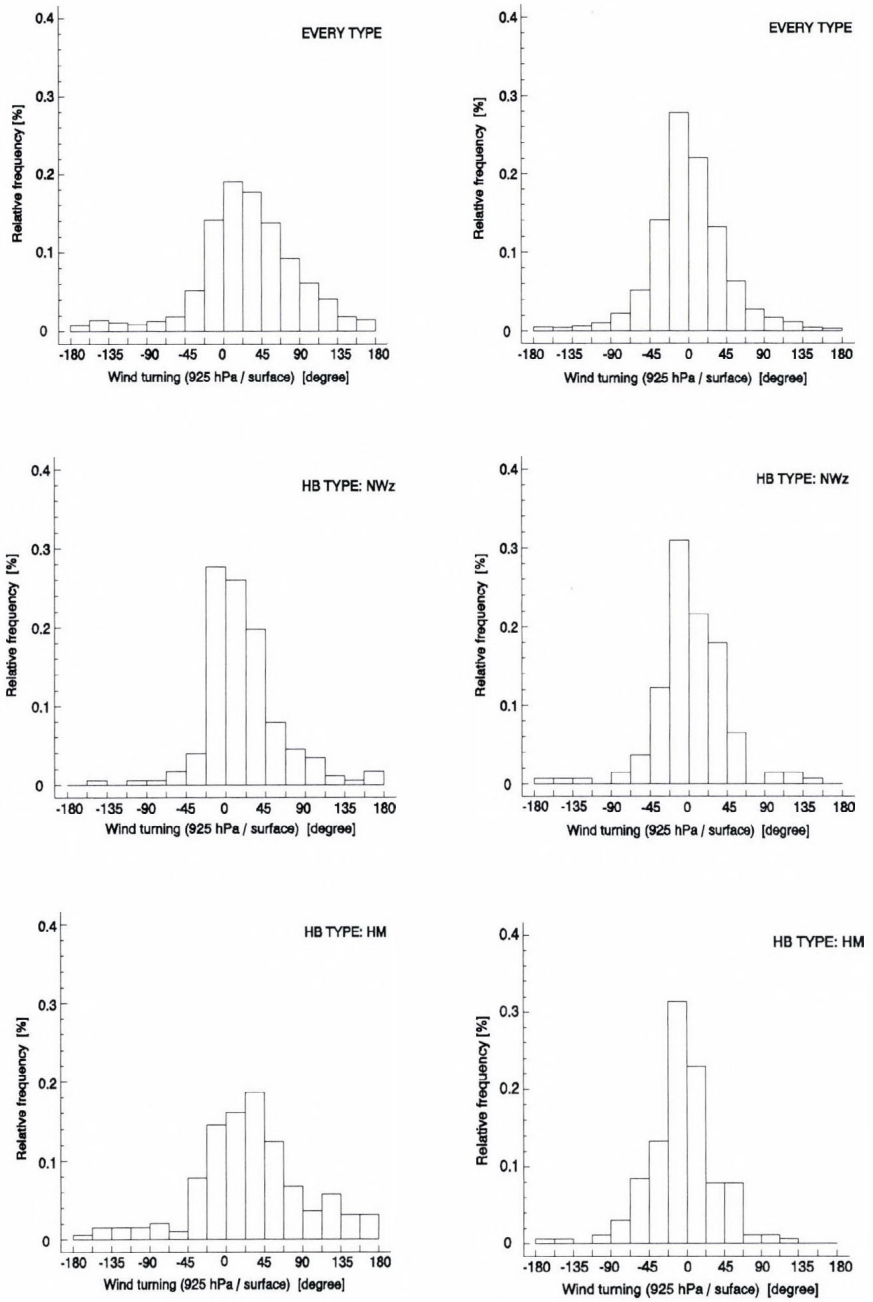

Fig. 4. Histogram of difference between wind directions (wind turning) at 925 hPa and surface levels in winter (left) and summer (right).

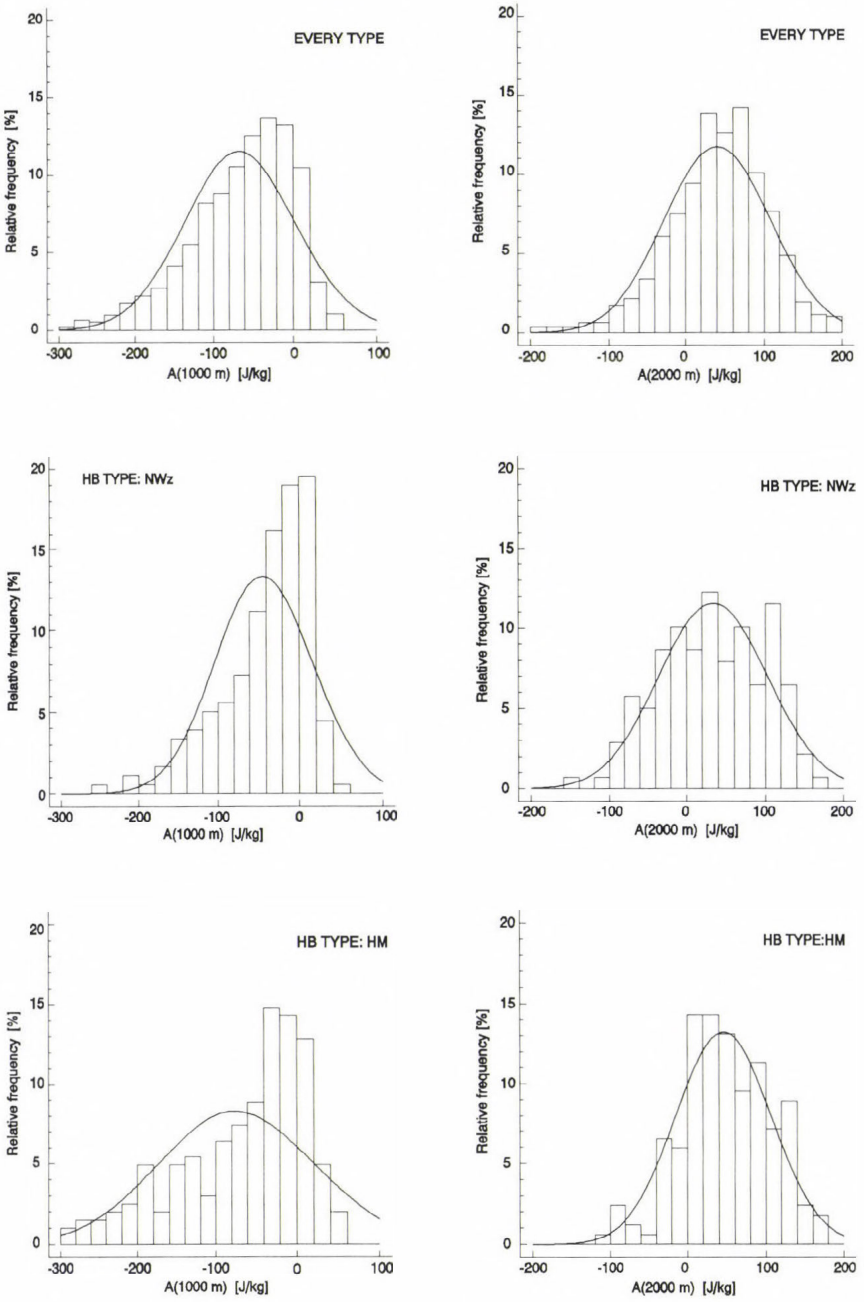

Fig. 5. Probability density of energy of instability in the lower 1km layer in winter (left) and in the lower 2 km layer in summer (right).

3. *Aggregating HB types*

3.1 Methodology

A hierarchical clustering technique has been defined in order to decrease by one the number of macrocirculation types in each step of the procedure. Let K denote the number of PBL characteristics and J denote the actual number of MC types. At the beginning of first step of the entire aggregation procedure the MC types are identical to HB types and J equals to 30. Then two MC types (HB types in the first step) are aggregated according to criteria described below and assigned to a new MC type. The rest of MC types remains unchanged and value of J decreases by one. This process is repeated until a prescribed number of MC types is achieved.

Two types are aggregated if

(a) The distance between these types is minimal.
In order to measure the distance between types i and j in terms of PBL characteristics we define the quantity

$$D_{ij} = \sum_{k=1}^{K} (m_{ik}/\sigma_{ik} - m_{jk}/\sigma_{jk})^2/(m_k/\sigma_k)^2, \qquad i,j = 1,...,J, \tag{2}$$

where subscripts i, j denote the conditioning on PBL parameters and k denotes the conditioning on MC types. m and σ correspond to mean and standard deviation, respectively. The numerator of Eq. (2) represents a Euclidian distance between means corresponding to types i and j with a normalization by their standard deviations. Denominator provides a further normalization in order to remove the differences between magnitudes of PBL parameters.

(b) Probability distributions of these types are similar.
Similarity of distributions is characterized by the chi-square distance

$$Q_{ij} = \sum_{k=1}^{K} n_i n_j \sum_{l=1}^{L} \frac{[(n_{ikl}/n_i) - (n_{jkl}/n_j)]^2}{n_{ikl} + n_{jkl}}, \qquad i,j = 1,...,J, \tag{3}$$

where n_i is the number of days in the MC type i, n_{ikl} is the number of data in the lth interval of histogram of the kth variable under MC type i, and L is the number of intervals (see e.g., *Dévényi* and *Gulyás*, 1988).

(c) Frequency of MC types is relatively uniform.

According to above considerations the aggregation procedure consists of the following steps.

(i) A few elements (5 %) of the matrix of Euclidian distances (Eq. (2)) having smallest distances is selected.

(ii) Three pairs of MC types having smallest values of the chi-square distance (Eq. (3)) are chosen from pairs of types obtained in (*i*).

(iii) Two MC types of that pair are aggregated from the three possibilities obtained in (*ii*) where the number of days in these two types is minimal.

(iv) Repeat steps (*i*)–(*iii*).

An experiment has been performed in order to examine sensitivity of aggregation procedure to changes of criteria (*i*)–(*iii*) and the result has been shown quite robust.

3.2. Results

The optimal number of MC types depends on the task in question and the sample sizes. In the actual case 8–12 MC types seem a good choice (*Fig. 6*). *Tables 3* and *4* show the main results for eight types.

Difference between PBL parameters in winter and summer is apparent. Evidently, winter generally has smaller PBL heights, smaller gradient of virtual temperature, stronger winds and negative energy of instability. A conjunctive use of the distance measure Eq. (2) and the similarity measure Eq. (3) of probability distributions of PBL parameters conditioned on different MC types seems a useful technique to reduce the number of HB types. For instance, the MC types MC1 and MC3 in summer have quite similar means of PBL parameters but with different probability distributions.

The HB types NWz and HM presented before are obviously found in different MC types in the two seasons. In winter the NWz Hess-Brezowsky type belongs to MC4, while the anticyclonic HM type is in MC2. The main characteristics of MC2 (Table 3) are similar to HM type: moderate virtual temperature gradient and wind speed, consequently high negative energy of instability. The mean PBL high is below the average. In summer, the NWz HB type forms alone an MC type (see MC5 in Table 4), and the anticyclonic HM type belongs to MC6.

In an earlier stage of the work (*Matyasovszky et al.*, 1996) the aggregation of HB types was performed without the energy of instability, and the structure of aggregated MC types was highly similar to the present case for each season and each step. For example, only 4 HB types were assigned to MC situation which differs from that of the previous case when using 8 MC types in summer. This is not surprising because the energy of instability is not independent statistically from the virtual temperature gradient and PBL height (see Table 1).

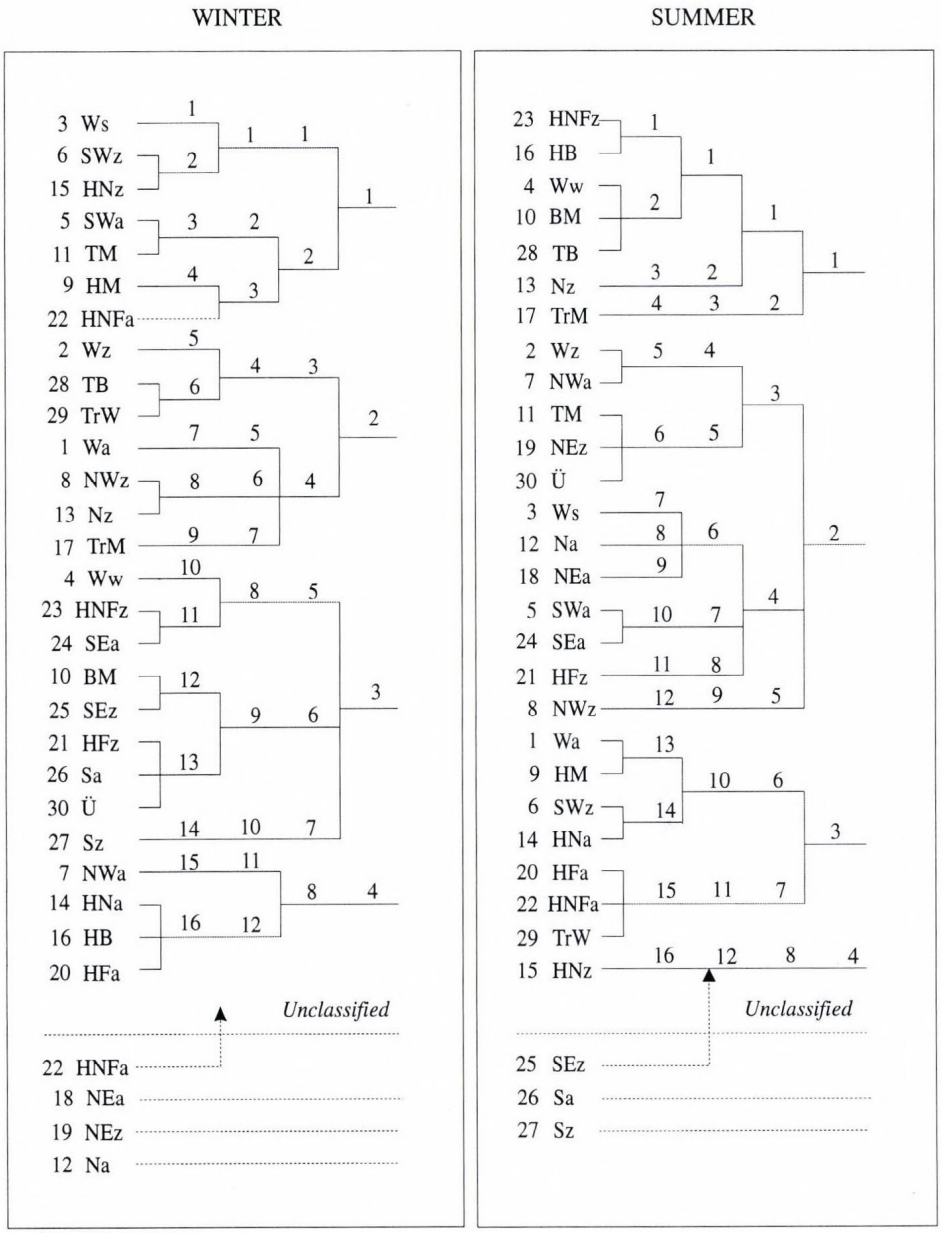

Fig. 6. The system of aggregated HB types for MC types of number of 16, 12, 8, 4. An MC type is unclassified when number of days in the type is smaller than 20.

Table 3. The distance matrix, relative frequency [%] of MC types, and mean of PBL parameters under the MC types in winter. (Numbers in bold indicate types where PBL parameters have different probability distributions at a 90% significance level.)

Type	1	2	3	4	5	6	7	8
1	0.00							
2	**0.18**	0.00						
3	**0.15**	**0.17**	0.00					
4	**0.20**	**0.25**	**0.24**	0.00				
5	**0.35**	**0.46**	**0.44**	**0.23**	0.00			
6	**0.26**	**0.33**	**0.35**	**0.15**	0.15	0.00		
7	0.39	0.49	0.43	**0.32**	**0.27**	**0.29**	0.00	
8	**0.64**	**0.71**	**0.72**	**0.49**	**0.31**	**0.40**	**0.49**	0.00
[%]	11	13	21	18	8	16	2	9
	(unclassified: 2%)							
H	504	585	577	415	559	611	464	719
γ	0.59	0.64	0.56	0.71	0.80	0.74	0.76	0.90
V	8.3	6.6	10.1	9.7	6.3	6.1	8.7	7.1
A	−84	−79	−80	−55	−62	−63	−89	−33

Table 4. The distance matrix, relative frequency [%] of MC types, and mean of PBL parameters under the MC types in summer. (Numbers in bold indicate types where PBL parameters have different probability distributions at a 90% significance level.)

Type	1	2	3	4	5	6	7	8
1	0.00							
2	**0.08**	0.00						
3	**0.17**	**0.18**	0.00					
4	**0.34**	**0.35**	**0.17**	0.00				
5	**0.23**	**0.24**	**0.13**	**0.21**	0.00			
6	**0.22**	**0.23**	**0.07**	**0.17**	**0.18**	0.00		
7	0.08	**0.12**	**0.12**	**0.30**	**0.19**	0.16	0.00	
8	**0.54**	**0.54**	**0.39**	**0.25**	0.33	**0.39**	**0.49**	0.00
[%]	23	5	22	12	5	19	11	2
	(unclassified: 1%)							
H	1361	1247	1396	1415	1296	1539	1410	1372
γ	1.15	1.09	1.15	1.13	1.09	1.18	1.15	1.09
V	5.0	6.6	6.1	5.3	7.0	4.7	4.7	5.5
A	39	11	39	44	34	46	45	39

4. Time series model of PBL characteristics

4.1 The model

To reproduce the simultaneous temporal statistical behavior of PBL parameters, a suitable model should be chosen. Autoregressive (AR) processes represent a well-developed and commonly used tool to model time series. They have been developed principally for Gaussian processes, but PBL parameters do not follow Gaussian distribution. Therefore, it is desirable to construct a transformation establishing a relationship between the distribution of the PBL parameters and the normal distribution. Time series of these hypothetical, normally distributed variables are modeled by AR processes and then the inverse of above mentioned transformation results in a time series model of PBL parameters. The temporal evolution of above mentioned hypothetical, normally distributed variables is modeled by first order autoregressive processes. The order of the model has been determined by Akaike's Information Criteria (*Akaike*, 1974).

As it was shown, the probability distribution is very different for different parameters and under different MC types, and therefore a simple analytical solution of the problem may not be expected. Therefore, one of the non-parametric techniques, the so-called Abramson method (*Abramson,* 1982) has been used to estimate probability distributions of PBL parameters. An important advantage of nonparametric methods is that they do not require assumptions on the shape of distribution functions. Details of these techniques are not discussed here, a climate oriented review of nonparametric probability density estimators can be found in *Matyasovszky* (1997).

4.2 Results

The entire data set is split into two parts and the stochastic model is developed from the first part of data. In order to validate the model, a time series of PBL parameters is simulated using the model, and several statistical characteristics of the second part of observed data and simulated data are compared. The main and standard deviation of PBL parameters are shown in *Table 5*. The stochastic model generally somewhat underestimates means in both seasons as well as standard deviations in summer. In winter, simulated standard deviations are larger than those observed except for wind speed and virtual temperature gradient. The model can reproduce not only simple characteristics like mean but probability distributions too. This is illustrated by *Fig. 7*.

In order to illustrate the accuracy of the stochastic model, another simulation experiment has been performed using the entire data set (without split sampling). In that case no visible difference can be recognized between observed and simulated probability distribution functions, which suggests that disagreements in *Table 6* or Fig. 7 are due to natural variability of PBL parameters, relative frequencies of HB types and data inhomogeneity, and not to model construction.

Table 5. Observed and simulated means and standard deviations of PBL parameters

Mean								
	Winter				Summer			
	H	γ_v	V	A	H	γ_v	V	A
Observed	628.6	0.71	7.9	-63.6	1442.1	1.16	5.4	40.6
Simulated	593.2	0.63	7.8	-71.9	1373.6	1.13	4.7	40.6
Standard deviation								
	Winter				Summer			
	H	γ_v	V	A	H	γ_v	V	A
Observed	390.3	0.47	4.7	66.8	630.6	0.29	3.3	71.1
Simulated	362.7	0.54	4.8	75.6	570.9	0.26	3.2	70.2

Table 6. Observed and simulated correlation matrices of PBL parameters with split sampling

Winter								
	Observed				Simulated			
	H	γ_v	V	A	H	γ_v	V	A
H	1.0	0.24	0.01	0.50	1.0	0.28	0.07	0.60
γ_v		1.0	-0.14	0.76		1.0	0.02	0.74
V			1.0	-0.04			1.0	0.09
A				1.0				1.0
Summer								
	Observed				Simulated			
	H	γ_v	V	A	H	γ_v	V	A
H	1.0	0.13	-0.08	0.28	1.0	0.12	-0.01	0.29
γ_v		1.0	-0.14	0.65		1.0	-0.03	0.64
V			1.0	-0.15			1.0	-0.04
A				1.0				1.0

The stochastic model reproduces the correlation matrices of PBL parameters quite well (Table 6). This is remarkable because the difference between correlations calculated from the entire data set (Table 1) and from the second half of data (Table 6) is not considerably smaller than the difference between correlations calculated from the second part of data and from simulated data.

Autocorrelations of PBL parameters decrease rapidly to zero, only one day lag values are significantly different from zero for both the observed and simulated series. For instance, one day lag autocorrelation of height of PBL was found 0.17 and 0.14 in winter and summer respectively. Corresponding simulated values are 0.17 and 0.16. The second remark is that correlation is not necessarily a best indicator of relationships between PBL parameters since the parameters are not distributed normally.

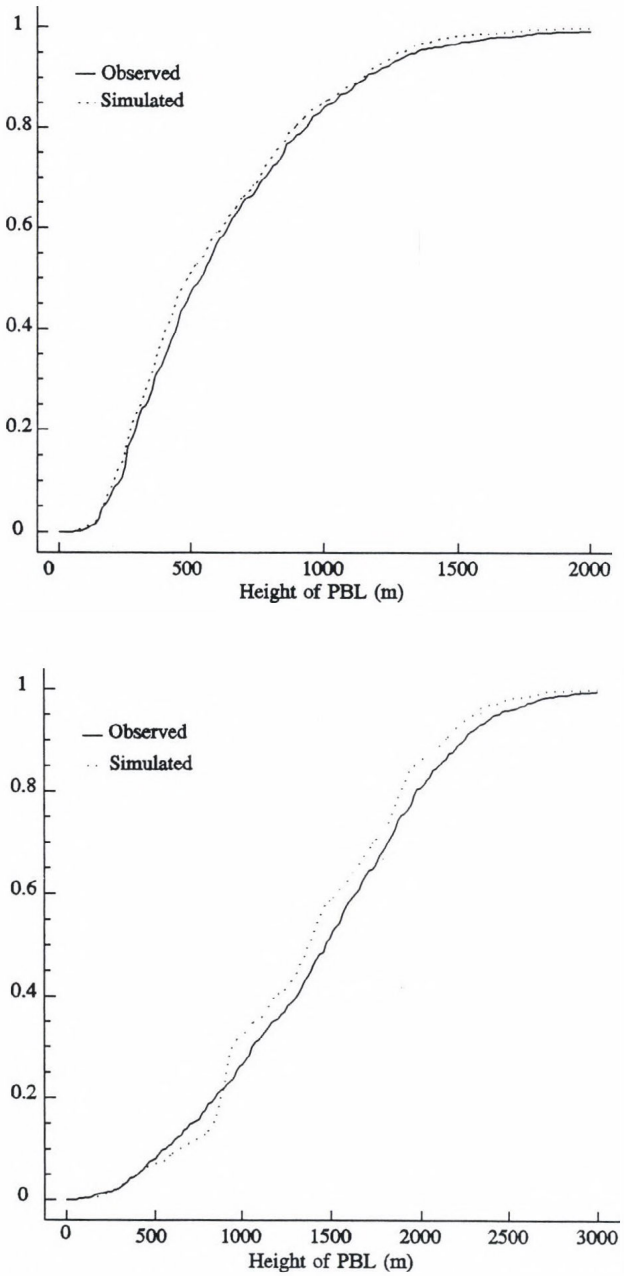

Fig. 7. Observed and simulated probability distribution functions of PBL height in winter (above) and summer (below).

5. *Conclusions*

The potential of the atmosphere to disperse and dilute pollutants depends upon various factors such as wind speed, height of PBL, vertical virtual temperature gradient, energy of instability, etc. Basic statistical characteristics of parameters controlling air pollution potential and their dependence on Hess-Brezowsky macrocirculation types have been presented in winter and summer seasons. The analysis has lead to the following conclusions:

- Statistical properties of PBL are well separated by HB types.
- The most suitable probability distribution for wind speed is frequently the lognormal distribution.
- The gradient of virtual potential temperature and energy of instability cannot be satisfactorily modeled by any well-known probability distribution.
- Calculation of the height of PBL using significant points of virtual temperature profile produces an uncertainty of 10–15 %, when the critical virtual temperature gradient is between 0.75°C/100 m and 0.85°C/100 m under the top of the PBL.
- The PBL height in different HB types can be adequately described by ordinary probability distributions.

A method has been developed in order to obtain a system of aggregated Hess-Brezowsky macrocirculation types in terms of characteristics controlling air pollution potential. Main conclusions can be summarized as follows:

- Correlations among the height of PBL, wind speed at the 925 hPa pressure level, and gradient of virtual temperature of the lower 300 m are quite low (≤ 0.3), thus, each parameter has an information essentially independent from information of the other variables. The energy of instability is statistically not independent from virtual temperature gradient of lower 300 m layer and from PBL height.
- The procedure developed for aggregating HB types is based on a conjunctive use of a distance measure of PBL parameters and a similarity measure of their probability distributions conditioned on MC types. The method provides an optimal choice for the number of days in the system of types.
- The technique resulted in statistically different conditional probability distributions of PBL parameters.

A multivariate time series model has been developed to describe simultaneous stochastic behavior of PBL parameters.

- The model reproduces satisfactorily observed statistical characteristics.
- Therefore, the model is suitable to simulate air pollution potential under hypothetical macrocirculation conditions.

It is intended to further develop and extend the stochastic model by incorporating pollutant concentrations.

Acknowledgements—Research leading to this paper has been supported by grant from Hungarian Science Foundation OTKA F-015493 and by grant from Higher Education Support Program FKFP-0193.

References

Abramson, I.S., 1982: On bandwidth estimation in kernel estimators — A square root law. *Ann. Statist. 10*, 1217-1223.

Akaike, H., 1974: A new look at the Statistical Model Identification. *IEEE Trans. Auto. Control. 19*, 716-723.

Bartholy, J. and *Kaba, M.*, 1987: Meteorological and statistical analyses and correction of the Hess-Brezowsky macrocirculation types (in Hungarian). *Országos Meteorológiai Szolgálat Kisebb Kiadványai, LVII.* Budapest, Hungary.

Bodolai, I., 1983: Main characteristics of the planetary boundary layer (in Hungarian). *Országos Meteorológiai Szolgálat Kisebb Kiadványai, LII.* Budapest, Hungary.

Dévényi, D. and *Gulyás, O.*, 1988: *Methods of Mathematical Statistics in Meteorology* (in Hungarian). Tankönyvkiadó, Budapest, Hungary.

Hess, P. and *Brezowsky, H.*, 1969: Katalog der Groswetterlagen Europas. *Ber. Deutsch. Wetterdienst*, Nr. 113, Bd. 15,2.

Matyasovszky, I., Weidinger, T. and *Németh, P.*, 1996: A system of aggregated Hess-Brezowsky macrocirculation types to characterize air pollution potential over Budapest. *Proceedings of Seventeenth International Conference on Carpathian Meteorology, Visegrád (Hungary) October 14-18, 1996*, 266-271.

Matyasovszky, I., 1997: Estimating probability density functions by kernel techniques. *Időjárás 101*, 17-31.

Stull, R.B., 1988: *An Introduction to Boundary Layer Meteorology*. Kluwer Academic Publishers, Dordrecht, Boston and London.

Szepesi, D., Popovics, M., Nárai, K., Iványi, Zs. and *Mersich, I.*, 1977: Meteorological simulation of urban air pollution. Part II. Diffusion climatological bases for the simulation of the transmission (in Hungarian). *Időjárás 81*, 129-146.

Weidinger, T., Matyasovszky, I. and *Németh, P.*, 1996: A statistical analyses of PBL over Budapest using macrocirculation types. *Proceeding of International Conference on Meteorological Processes in the Boundary Layer of Atmosphere, 1996. Stara Lesná, Slovakia, October 7-11, 1996*, 188-193.

Wiswanadham, D.V. and *Santosh, K.R.*, 1989: Air pollution potential over South India. *Boundary-Layer Meteorology 48*, 299-313.

IDŐJÁRÁS

Quarterly Journal of the Hungarian Meteorological Service
Vol. 102, No. 4, October–December 1998, pp. 239–246

Some aspects of the urban heat island and relative humidity in larger Belgrade area

Miroslava Unkašević

Department of Meteorology, Faculty of Physics, University of Belgrade, Dobračina 16, 11001 Belgrade, Yugoslavia; E-mail: itosic@afrodita.rcub.bg.ac.yu

(Manuscript received 23 March 1998; in final form 24 July 1998)

Abstract—This paper presents the investigation of the urban effects on the monthly mean values of the minimum temperature and relative humidity in the area of Belgrade. The minimum urban temperature increase is explained by linking the temperatures with resident population, a parameter that reflects the size of the city itself. This examination indicates that urban air contains less relative humidity than suburban and rural ones.

Key-words: heat island, relative humidity, Belgrade area.

1. Introduction

Urbanization and industrialization have resulted in the modification of the local climate of many cities. This modification, in general, involves the alteration of the local energy and atmospheric moisture budget.

The existence of the urban heat island is usually explained as the effect of the city itself on the energy balance and the artificial heat added by combustion processes in residential and industrial buildings.

Urban-rural temperature differences are well documented, as is the heat island structure of the build-up areas as a whole (*Preston-Whyte*, 1970; *Nkemdirim*, 1976; *Goldreich*, 1985). *Voogt* and *Oke* (1997) used ground and airborne thermal infrared radiometers to estimate the surface temperature of urban areas. Many authors concluded that few studies make comparison between urban and their rural surroundings relative humidity values (*Hage*, 1975; *Kawamura*, 1985; *Brazel* and *Balling*, 1986; *Ackerman*, 1987; *Lee*, 1991).

Hage (1975) found that in winter the relative and absolute humidity were high in the city at any time because of vertical mixing and combustion sources. *Kawamura* (1985) and *Brazel* and *Balling* (1986) concluded that various

activities and landscapes associated with urbanization can be ultimate force of a kind urban "humidity island" effect. *Ackerman* (1987) suggested that urban vapour pressure and dew points were lower than the rural ones only in the forenoon and spring afternoons.

Lee (1991) concluded that in London the urban atmosphere was more humid than the rural at night in all months and during the day in winter and spring, while during summer days, the urban atmosphere was less humid.

The Belgrade basin with an estimated population of 2.0 million in 1991 covers approximately 3221 km^2 area with the fairly high mountain Avala to the south and lowlands to the north and west. The climate of Belgrade is continental in character. The Meteorological Station of the Belgrade Observatory which is situated at 132 m above mean sea level is the basic station for the analysis of the monthly mean values of minimum temperature and relative humidity.

Strong industrial zone in the Belgrade city is concentrated along coastal rivers Sava and Danube (*Fig. 1*), while commercial district and dense buildings are concentrated around the Belgrade Observatory Station. Residential areas with parks are located on highest parts of the area of Belgrade.

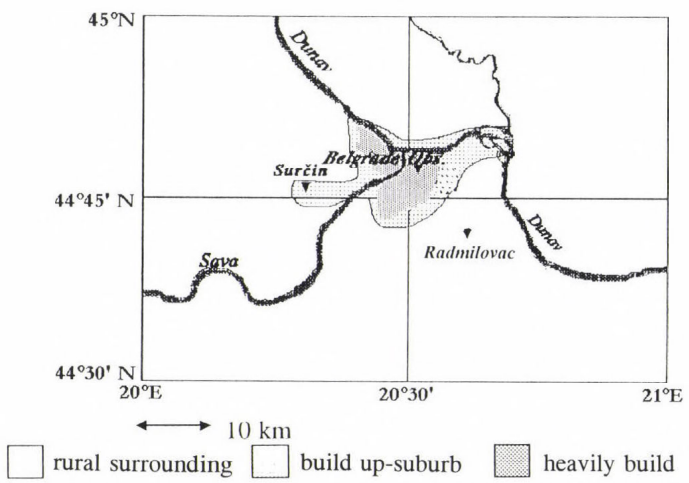

Fig. 1. Map of the Belgrade area showing the next stations:
1. Belgrade Observatory (urban), 2. Surčin Airport (suburban) and 3. Radmilovac (rural).

The daily measurements of the minimum temperature are carried out at the next location: Belgrade Observatory (urban), Surčin Airport (suburban) and Radmilovac (rural) for the period 1970–1991. The monthly mean values of the minimum temperature are determined using the daily values.

For each mean value the standard deviation has been also calculated in order to verify the data according to the ordinary criteria of the statistical distributions, e.g., the t-distribution tables with $n-1$ degree of freedom (since the standard deviation is obtained from $n \geq 30$). Besides, the Kolmogoroff-Smirnoff homogeneity test was carried out and adjustments were made to filter out inhomogeneities due to errors introduced by instruments and observed changes.

Elevations between the Belgrade Observatory (132 m), Surčin Airport (96 m) and Radmilovac (130 m) differ maximally about 36 m, so the possible effect of station elevation on the diurnal temperature range is negligible (*Kuttler et al.*, 1996).

The present report is the result of recent research of the mean magnitude of the urban heat island (1970–1991) and the humidity island (1970–1991 and 1976–1980).

2. The urban heat island

The presence of the heat island appears more strongly in the minimum temperatures than in the mean and maximum temperatures (*Landsberg*, 1970; *Oke*, 1974, 1979; *Colacino* and *Lavagnini*, 1982). It may be explained by physical mechanisms which define the next effects:

(1) Increased counter radiation due to absorption of outgoing long-wave radiation and remission by polluted urban atmosphere.
(2) Greater day-time heat storage due to the thermal properties of urban materials and its nocturnal release.
(3) Anthropogenic heat from building sides and fabrics.
(4) Decreased evaporation due to the removal of vegetation.
(5) Decreased loss of sensible heat due to the reduction of wind speed in the city.

Anthropogenic heat from building sides have a maximum in the winter season. In summer it would seem possible that effects of 1, 2 and to lesser extent 3, 4 and 5 may combine to make the city store the sensible heat by day and hence keep urban temperature higher than in the countryside (*Grimmond* and *Oke*, 1995).

It is obvious from *Fig. 2* that the mean urban minimum temperature is always higher than the suburban (Fig. 2a) and rural (Fig. 2b) ones. The maximum frequency distribution of ΔT_m (monthly mean minimum temperature difference between the urban and suburban/rural stations) are related to the temperature intervals from 1.5 to 2.5°C for the suburban (Fig. 2a) and from 2.5 to 3.5°C for the rural station (Fig. 2b).

Despite the fact that the urban heat island morphology is strongly controlled by the unique character of each city, it seems reasonable to suggest the mean magnitude of the heat island is at least 2–3°C.

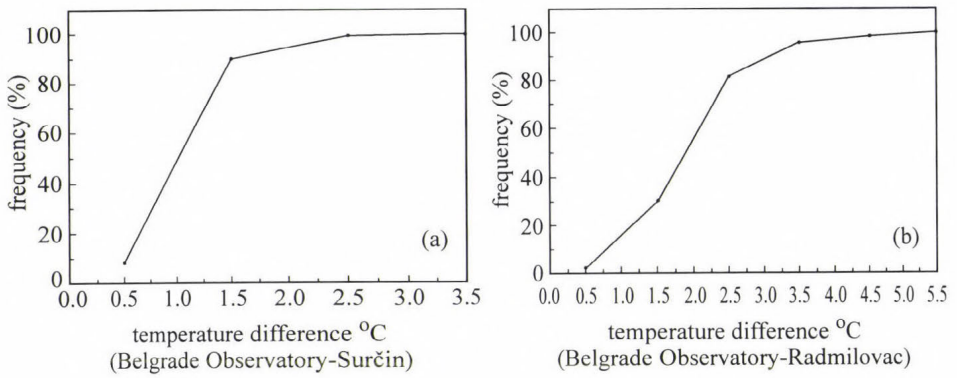

Fig. 2. Cumulative frequency distribution of the monthly mean minimum: (*a*) urban-suburban and (*b*) urban-rural temperature difference during the period 1970–1991.

The examined period (1970-1991) corresponds to the period of maximum development of the city and so it is particularly suitable for checking the validity of some formulae relating temperature variations to urban development (*Landsberg*, 1981). The minimum urban temperature increase is usually explained by linking the temperatures with resident population, a parameter that reflects the size of the city itself. For Belgrade, the statistical correlation analysis was carried out using annual data referring to the resident population (P) from 1890 until 1990, together with the corresponding minimum temperatures T_m measured at Belgrade Observatory (*Fig. 3*). The obtained result is generally similar to the result obtained by *Katsoulis* (1987), who examined long term climatic change of air temperature in Athens. Regression was carried out using the next relation:

$$T_m = 8.15 + 0.03 \log P. \tag{1}$$

This form of equation does not allow the identification of critical wind speed at which urban heat island obliterated. If winds are included, the relation between the maximum heat island (ΔT_{u-r}) and the population is given by (*Oke*, 1974):

$$\Delta T_{u-r} \approx P^{1/4}/4\,\bar{u}^{1/2} \tag{2}$$

where $\bar{u}$ is regional (non-urban) mean wind speed at a height of 10 m. Based on observations in the vicinity of Belgrade (2 million inhabitants) it appears that

this value is approximately 10 m s^{-1} in the case of "Koshava" wind (the most frequent, moderate to strong wind in greater Belgrade area).

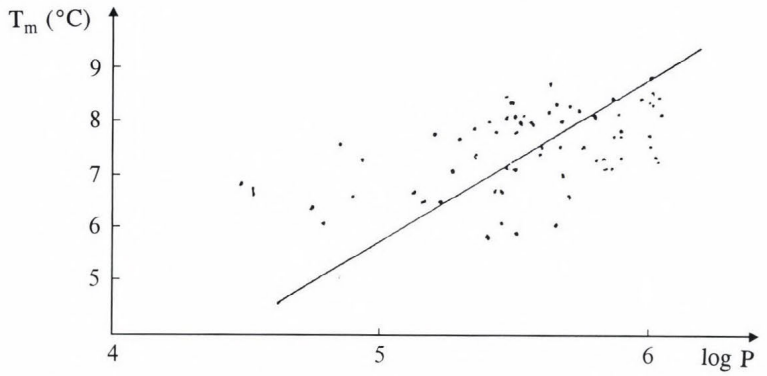

Fig. 3. Correlation between annual mean minimum temperature and log *P* (*P* is population number) for Belgrade Observatory during 1890-1990.

3. Some investigation of the relative humidity in Belgrade

In Belgrade, winter air is moist and summer air is dry, although in winter air contains less water vapour than in summer. *Table 1* presents the hourly mean (06, 13 and 20 UTC) and the monthly mean values of the relative humidity (%) measured at Belgrade Observatory during the period of 1970–1991. The monthly mean values of the relative humidity in Table 1 shows that the relative humidity decreases from winter toward summer months. Slight increase of the relative humidity recorded in June is caused by maximum precipitation which occurring in Belgrade in June.

Table 1. Averaged hourly and monthly mean values of the relative humidity (%) in Belgrade during the period 1970-1991

UTC	Jan	Feb	Mar	Apr	May	Jun	Jul	Aug	Sep	Oct	Nov	Dec
6	80	79	77	71	73	75	73	74	77	82	84	79
13	70	64	55	49	52	52	48	46	50	55	68	76
20	78	76	69	66	70	71	68	69	74	76	70	80
Mean	**76**	**73**	**67**	**63**	**65**	**66**	**63**	**63**	**67**	**72**	**78**	**78**

Table 1 also shows that although the minimum mean monthly temperature is recorded in January, the maximum of the relative humidity occurs in December.

Daily variations of the relative humidity in the summer months are about twice bigger than in the winter months. Because of these changes the air in Belgrade is frequently dry on summer days.

The averaged seasonal values of the relative humidity (RH) measured at Belgrade Observatory during the period 1970–1991 are:

	Winter	Spring	Summer	Autumn
Seasonal value RH (%)	76	66	64	74
Seasonal variance RH (%)	14	24	27	24

From these values of the relative humidity we can conclude that the relative humidity in autumn is 8% more than in spring, although the averaged seasonal temperature in autumn is higher than in spring. However, the averaged seasonal variances of the relative humidity are the same during spring and autumn.

The Student's t-test indicates that December, January and February have been characterized by a sharp decrease in the relative humidity levels in the period 1970–1991 according to the period 1925–1969 (*Unkašević*, 1996). This analysis suggests that such large drops in the relative humidity during the cold season must be associated with the urban heat island. This is a reflection of the strong inverse relationship of relative humidity to temperature, and thus of the relationship between ΔRH_{u-r} and ΔT_{u-r}. ΔRH_{u-r} is related to the relative humidity differences between the urban and rural sites.

In this study, suburban/rural-urban relative humidity differences at fixed hours (06, 13 and 20 UTC) during the period 1976–1980 have been used. It is obvious from *Fig. 4* that the urban air containes less relative humidity than suburban and rural air. The frequency distributions for suburban/urban-rural relative humidity differences are shifted to positive values, i.e., toward higher relative humidities in the suburban and rural areas. The reverse is true in less than 11% and 17% of the measurements at 06 UTC at the suburban and rural stations, respectively. Measurements of the relative humidity at 13 UTC indicate that this difference has an almost unchanged frequency in suburban and increased frequency in rural areas. Namely, the frequency distribution for ΔRH is shifted to negative values in less than 18% and more than 32% at 13 UTC at the suburban and rural stations, respectively. The frequency distribution at 20 UTC and on the daily basis have many of the same features as at 06 UTC.

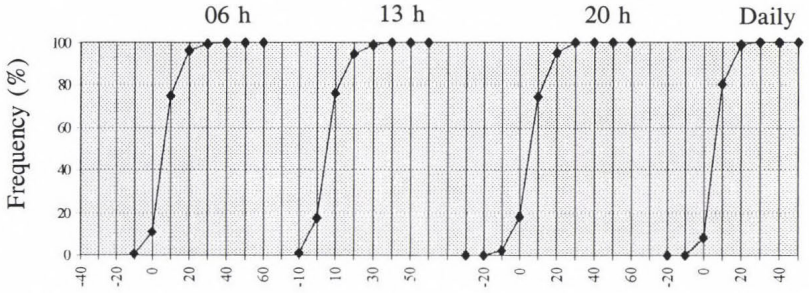

(a) Relative humidity difference (Surčin–Belgrade Observatory)

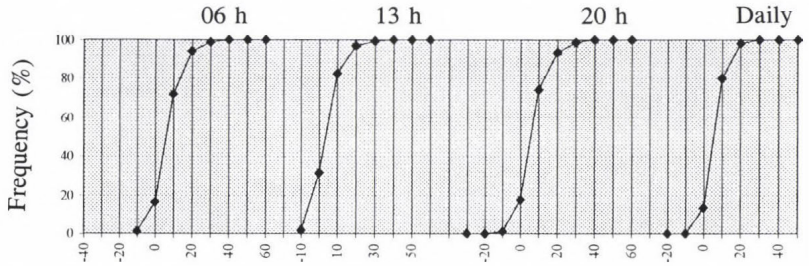

(b) Relative humidity difference (Radmilovac–Belgrade Observatory)

Fig. 4. Cumulative frequency distribution of the hourly mean (06, 13, 20 UTC) and daily mean: (*a*) suburban-urban and (*b*) rural-urban relative humidity differences (ΔRH %) during the period 1976–1980.

4. Conclusions

Increased heating activities in the Belgrade city (more use of central heating, air conditioning, release of energy by industrial activity and traffic) substantially raised the air temperature above the city. It was shown that the monthly mean values of minimum urban temperature is always higher than the suburban and rural ones. Effect of the heat island is explained by a 2–3 °C increase of the mean minimum temperature.

Regression analysis results obtained for the correlation between the yearly mean minimum urban temperature and population number in Belgrade follow the logarithmic model.

The relative humidity was usually lower in the city than in the surrounding areas and the urban-rural relative humidity difference were strongly affected by the urban heat island.

References

Ackerman, B., 1987: Climatology of Chicago area urban-rural differences in humidity. *J. Clim. Appl. Meteor. 26*, 427-730.

Brazel, W.S. and *Balling, R.J.*, 1986: Temporal analysis of long term atmospheric moisture levels in Phoenix, Arizona. *J. Clim. Appl. Meteor. 25*, 112-117.

Colacino, M. and *Lavagnini, A.*, 1982: Evidence of the urban heat island in Rome by climatological analysis. *Arch. Meteor. Geophys. Bioklim.*, B21, 87-97.

Goldreich, Y., 1985: The structure of the groundlevel heat island in a central business district. *J. Clim. Appl. Meteor. 24*, 1237-1244.

Grimmond, C.S. and *Oke, T.R.*, 1995: Comparison of heat fluxes from summer time observations in the suburbs of four north American cities. *J. Appl. Meteor. 34*, 873-889.

Hage, K.D., 1975: Urban-rural humidity differences. *J. Appl. Meteor. 14*, 1277-1283.

Katsoulis, B., 1987: Indication of change of climate from the analysis of air temperature time series. *Climatic Change 10*, 67-79.

Kawamura, T., 1985: Urban-rural humidity differences in Japan. *Geop. Review Japan 58*, 83-94.

Kuttler, W., Barlay, A. and *Rosmann, F.*, 1996: Study of the thermal structure of a town in a narrow valley. *Atmosph Environment 30*, 365-378.

Landsberg, H.E., 1970: Climates and urban planning. Urban climates. *Techn. Paper 141, WMO*, Geneva, 364-374.

Landsberg, H.E., 1981: *The Urban Climate*. Int. Geophys. Ser. 28, Academic Press, 261 pp.

Lee, D.O., 1991: Urban-rural humidity differences in London. *Int. J. Climatol. 11*, 577-582.

Nkemdirim, L.C., 1976: Dynamics of an urban temperature field-A case study. *J. Appl. Meteor. 15*, 818-828.

Oke, T.R., 1974: Review of urban climatology. *WMO, Techn. Note 134*, WMO, Geneva, 132 pp.

Oke, T.R., 1979: Review of urban climatology. *WMO, Techn. Note 169*, WMO, Geneva, 114-119.

Preston-Whyte, R.A., 1970: A spatial model for an urban heat island. *J. Appl. Meteor. 9*, 571-573.

Unkašević, M., 1996: Analysis of atmospheric moisture in Belgrade, Yugoslavia. *Meteor. Zeit. 3*, 121-124.

Voogt, J.A. and *Oke, T.R.*, 1997: Complete urban surface temperatures. *J. Appl. Meteor. 36*, 1117-1131.

IDŐJÁRÁS

Quarterly Journal of the Hungarian Meteorological Service
Vol. 102, No. 4, October–December 1998, pp. 247–257

Radiative cooling rate in the atmospheric boundary layer

František Smolen and **Marian Ostrožlík**

Geophysical Institute of Slovak Academy of Sciences
Dúbravská cesta 9, 842 28 Bratislava, Slovak Republic
E-mail: geofostr@savba.sk

(Manuscript received 8 September 1998)

Abstract—The long-wave radiation flux density measurements at the meteorological observatories Skalnaté Pleso (φ = 49°12'N, λ = 20°14'E, H = 1778 m a.s.l.) and Stará Lesná (φ = 49°09'N, λ = 20°17'E, H = 810 m a.s.l.) in High Tatras during the period 1991–1995 were used to study the radiative temperature changes in the atmospheric boundary layer.

Based on the changes of the long-wave radiation balance with altitude in the atmospheric layer between Stará Lesná and Skalnaté Pleso, the fluctuations of the radiative cooling rates were calculated. The effects of the thermal atmospheric stratification and the water vapor content on the radiative cooling or heating rates were determined. A special attention was paid to the daily and seasonal courses, as well as to the effect of clouds.

Key-words: radiative temperature changes, radiative cooling, radiative heating, radiative cooling rate, long-wave radiation balance, long-wave radiation flux density, thermal atmospheric stratification, atmospheric boundary layer.

1. Introduction

The atmosphere losses energy by emission of infrared radiation toward the space and toward the surface. Except for ozone, the primary long-wave radiation absorbing gases cool the atmosphere. The water vapor dominates the long-wave cooling in the troposphere. The radiative cooling rate depends in a large extent upon the cloudiness, the thermal stratification as well as on the water vapor content in the atmosphere. The concentration of other greenhouse gases in the atmosphere plays an important role, too. *Timanovskaja* and *Faraponova* (1967) have shown that the radiative cooling rate can be about 5 K h^{-1} during night-time as a consequence of the long-wave radiation flux divergence in the atmospheric ground layer, and on the other hand, during the

daylight time the radiative heating can lead to rate of 6 K h^{-1} by the long-wave radiation absorption.

To study the radiative temperature changes of the atmosphere, both the solar energy transfer and the long-wave radiation transfer should be taken into account. Comparison of the results obtained by the different calculation methods has shown that the difference between them can be up to 50 per cent in some cases (*Goody*, 1964).

The purpose of this paper is to find empirical dependence of radiative cooling on cloudiness as well as on thermal atmospheric stratification. A special attention is paid to study the effect of the low clouds on the radiative cooling rate in the boundary layer of atmosphere.

2. *Material and methods*

Long-wave radiation flux measurements, which have been used as input parameters at the study of radiative cooling rate, were carried out at the mentioned observatories during the period 1991–1995. The suitable positions of these two close sites with different altitude (the difference is about 1000 m) enabled us to study the vertical and seasonal variations of radiative cooling and heating in the boundary layer of atmosphere.

To measure the long-wave radiation fluxes, Schulze's radiation balance meters were used. They were located at 1.5 m height over the active surface. Simultaneously with the long-wave radiation flux measurements, the air temperature, air humidity and air pressure were measured, and the amount and type of clouds were observed (*Ostrožlík* and *Janičkovičová,* 1992–1995). To calculate the radiative cooling rate in the atmospheric boundary layer, the vertical changes of long-wave radiation balance $\Delta F/\Delta z$ were used.

On the basis of the long-wave radiation balance differences (ΔF) between the levels Stará Lesná and Skalnaté Pleso the radiative cooling rate $(\delta T/\delta t)_{\Delta F}$ can be calculated. To calculate this rate we used the following relationship

$$\left(\frac{\delta T}{\delta t}\right)_{\Delta F} = -\frac{1}{c_p \rho}\,\frac{\Delta F}{\Delta z}, \tag{1}$$

where T is air temperature, t is time, z is altitude, c_p is the specific heat capacity at constant pressure, ρ is the air density and $\Delta F/\Delta z \cong \text{div } F$.

3. Results

3.1 Time variability of net flux

Figs. 1 and *2* represent the daily and seasonal variability of the long-wave radiation balance at the observatories Stará Lesná and Skalnaté Pleso. Basic characteristics of the curves in these figures show good coincidence with the results of many authors (*Kondratyev et al.*, 1972; *Prokofjev* and *Ter-Markarjanc*, 1972; *Rodgers*, 1967; *Stephens et al.*, 1994; *Zajceva* and *Šljachov*, 1972).

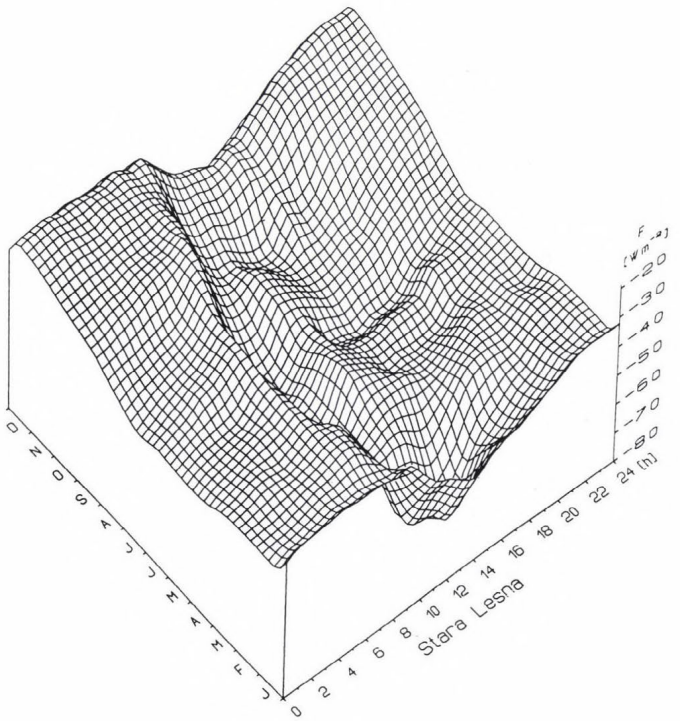

Fig. 1. Daily and seasonal variations of the long-wave radiation balance (F) in W m^{-2} at Stará Lesná during the period 1991–1995.

The net terrestrial radiation increases with altitude. Numerical results show that while the absolute value of F is 41.68 W m^{-2} at Stará Lesná, its value increases at Skalnaté Pleso up to 58.14 W m^{-2} in annual average. At clear sky (amount of clouds is less than 2/10 at both places) the corresponding values are 66.60 W m^{-2} at Stará Lesná, and 95.56 W m^{-2} at Skalnaté Pleso. The greatest

values of F occur at clear sky in March when the mean daily value of the long-wave radiation balance is 82.50 W m^{-2} at Stará Lesná and 117.23 W m^{-2} at Skalnaté Pleso. Based on these results we can state that the actual thermal energy loss owing to the long-wave radiation fluxes in the atmosphere is in average about 30 per cent higher at Skalnaté Pleso than at Stará Lesná.

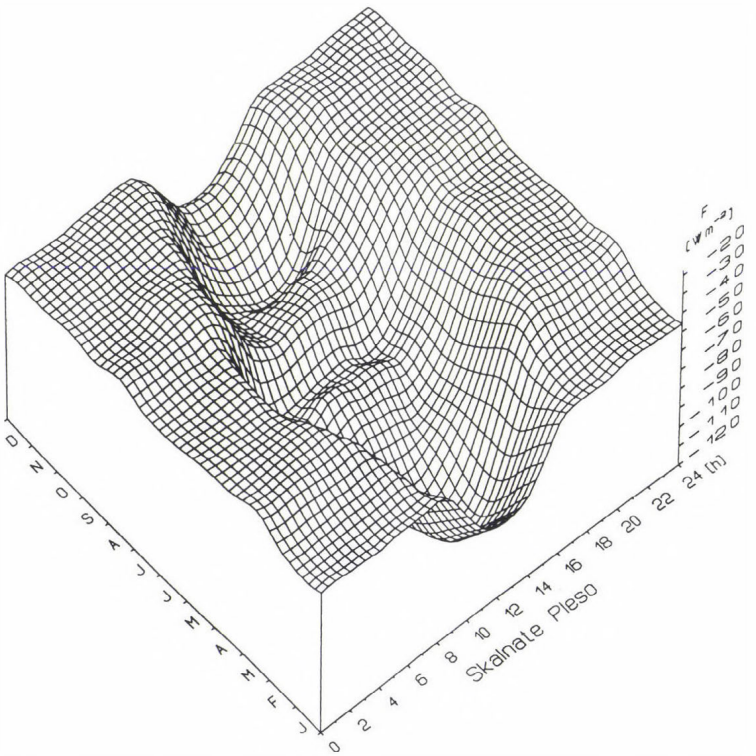

Fig. 2. Daily and seasonal variations of the long-wave radiation balance (F) in W m^{-2} at Skalnaté Pleso during the period 1991–1995.

Some anomalies in vertical changes of long-wave radiation balance during the day can be seen from February to October in evening hours after sunset. In this part of day the absolute values of F at Skalnaté Pleso are smaller than at Stará Lesná. This anomaly is caused by the fact that the downward atmospheric radiation changes slower than the radiation emitted by the active surface.

The actual thermal energy loss in the atmospheric layer between Stará Lesná and Skalnaté Pleso, expressed as a difference of the long-wave radiation balance ΔF, is illustrated on *Fig. 3*.

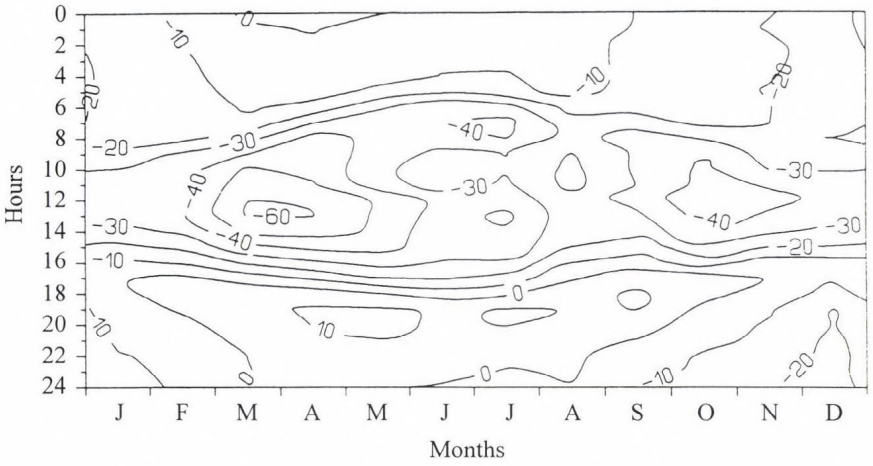

Fig. 3. Thermal energy loss in the atmospheric layer between Stará Lesná and Skalnaté Pleso as a difference of the long-wave radiation balance (ΔF) in W m^{-2} during the period 1991–1995.

3.2 Radiative temperature changes

Radiative temperature change can be expressed by the following relation: if $\Delta F/\Delta z < 0$ then $(\delta T/\delta t)_{\Delta F} > 0$, on the other hand if $\Delta F/\Delta z > 0$ then $(\delta T/\delta t)_{\Delta F} < 0$. In the first case radiative cooling, in the second one radiative heating occurs. When $\Delta F/\Delta z = 0$ then radiation equilibrium exists (*Kondratyev*, 1956).

Time variability of the radiative temperature changes $(\delta T/\delta t)_{\Delta F}$ in the atmospheric layer between Stará Lesná and Skalnaté Pleso under average cloud condition is illustrated on *Fig. 4*. The corresponding values of $(\delta T/\delta t)_{\Delta F}$ at clear sky (cloud amount is less than 2/10 at both localities) are presented on *Fig. 5*. From the comparison of the individual data we can see that the occurrence of clouds in the atmosphere causes a decrease of the radiative cooling. As average, in 43% of the days clouds occur in the layer between Stará Lesná and Skalnaté Pleso. *Stephens et al.* (1994) introduce that the clouds in relatively moist regions decrease the radiative cooling almost to the half of the clear sky values. The most intensive radiative cooling in the investigated atmospheric boundary layer can be seen in December. At average cloudiness the daily mean of $(\delta T/\delta t)_{\Delta F}$ is 0.097 K h^{-1}, at clear sky it is 0.167 K h^{-1}.

In a coincidence with results of *Prokofjev* and *Ter-Markarjanc* (1972) the most intensive radiative cooling occurs at the midday. In this part of day in March and April the mean values of $(\delta T/\delta t)_{\Delta F}$ vary between 0.237 K h^{-1} and 0.246 K h^{-1} at mean cloud conditions and in the range of 0.351 K h^{-1} and 0.583 K h^{-1} at clear sky.

In the evening hours from February to October the values of $\Delta F/\Delta z$ in the layer between Stará Lesná and Skalnaté Pleso are greater than zero. The radiative heating of the atmospheric boundary layer occurs as a consequence of long-wave radiation absorption. This effect is more expressive at mean cloud conditions than at clear sky.

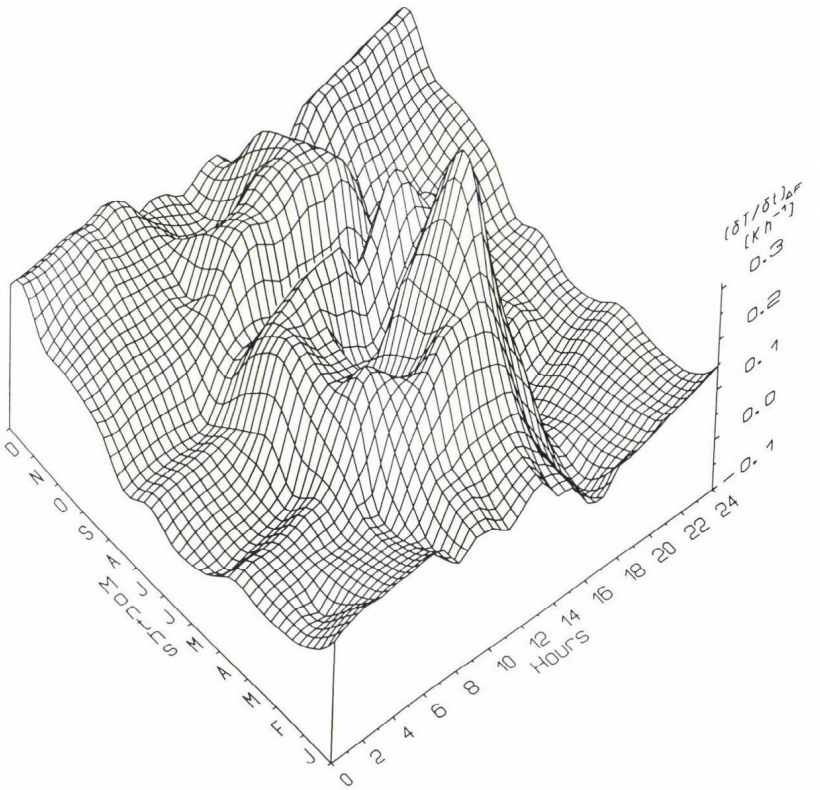

Fig. 4. Daily and seasonal variations of the radiative temperature changes $(\delta T/\delta t)_{\Delta F}$ in K h^{-1} at the average cloud conditions in the atmospheric layer between Stará Lesná and Skalnaté Pleso during the period 1991–1995.

More detailed analysis of the daily course of radiative cooling confirmed that the radiative cooling rate depends in a substantial measure on the thermal stratification of the investigated atmospheric layer. This dependence is clearly illustrated on *Fig. 6.* As we can see from Fig. 6 the values of $(\delta T/\delta t)_{\Delta F}$ rise with the increasing atmospheric stability. The greatest radiative cooling rate corresponds to strong thermal inversion. On the other hand at unstable atmospheric stratification when the vertical air temperature gradient is in the range of 1.01–1.60°C/100 m, radiative heating occurs in the atmospheric layer

between Stará Lesná and Skalnaté Pleso at both average cloud coverage and overcast sky. Radiative equilibrium occurs when the thermal gradient is in the range of 1.01–1.20°C/100 m. The greatest fluctuation of $(\delta T/\delta t)_{\Delta F}$ exists at the unstable atmospheric stratification. This fact can be caused by the convective as well as the turbulent transfer of water vapor.

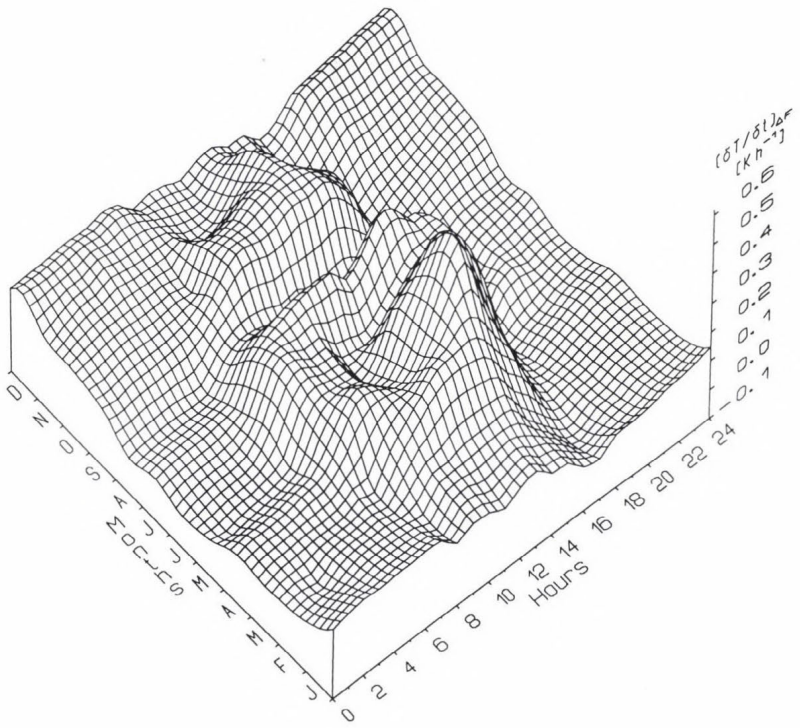

Fig. 5. Daily and seasonal variations of the radiative temperature changes $(\delta T/\delta t)_{\Delta F}$ in K h^{-1} at the clear sky in the atmospheric layer between Stará Lesná and Skalnaté Pleso during the period 1991–1995.

Functional dependence of the radiative cooling rate on the vertical change of air temperature *(dT/dz)* in the observed layer can be expressed by polynomial of degree 3

$$\left(\frac{\delta T}{\delta t}\right)_{\Delta F} = a_0 + a_1\frac{dT}{dz} + a_2\left(\frac{dT}{dz}\right)^2 + a_3\left(\frac{dT}{dz}\right)^3. \qquad (2)$$

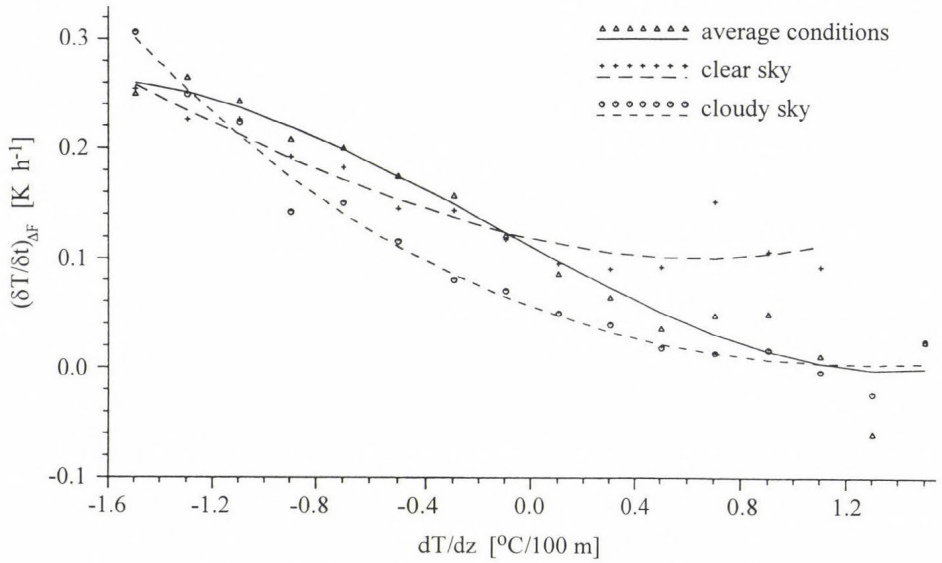

Fig. 6. Dependence of the radiative temperature changes $(\delta T/\delta t)_{\Delta F}$ in K h^{-1} on the thermal atmospheric stratification (dT/dz) in °C/100 m at the different cloud conditions in the atmospheric layer between Stará Lesná and Skalnaté Pleso during the period 1991–1995. The curves correspond to polynomial of the third degree.

The values of the regression coefficients a_0, a_1, a_2, a_3 are listed in *Table 1*.

Table 1. Coefficients a_0, a_1, a_2, a_3 of Eq. (2), and correlation coefficient (r) between experimental and calculated values

Cloud conditions	Coefficients				
	a_0	a_1	a_2	a_3	r
Clear sky	0.1179	–0.0538	0.0362	0.0064	0.9491
Overcast sky	0.0554	–0.0888	0.0433	–0.0047	0.9907
Average conditions	0.1106	–0.1287	0.0084	0.0185	0.9777

The dependence of the radiative cooling rate $(\delta T/\delta t)_{\Delta F}$ on the water vapor pressure (e) in the layer between Stará Lesná and Skalnaté Pleso is presented in graphical form on *Fig. 7*. From the course of the curves on this figure we can see that in average the radiative cooling rate decreases with the rise of the water vapor pressure. There is a substantial, more complicated situation when the sky is clear (curve 2 on Fig. 7). This dependence is characterized by two

maxima. The expressive increase of the quantity $(\delta T/\delta t)_{\Delta F}$ occurs at the water vapor pressure from 0.1 to 4.0 hPa. Later, at the further rise of the water vapor pressure till to 8 hPa, the values of $(\delta T/\delta t)_{\Delta F}$ begin suddenly decrease. Over this value we can see the slow linear rise of the radiative cooling rate and then its decrease in the atmospheric boundary layer. This dependence of $(\delta T/\delta t)_{\Delta F}$ on the water vapor pressure at the clear sky indicates the complication of this problem, which will require a more detailed analysis.

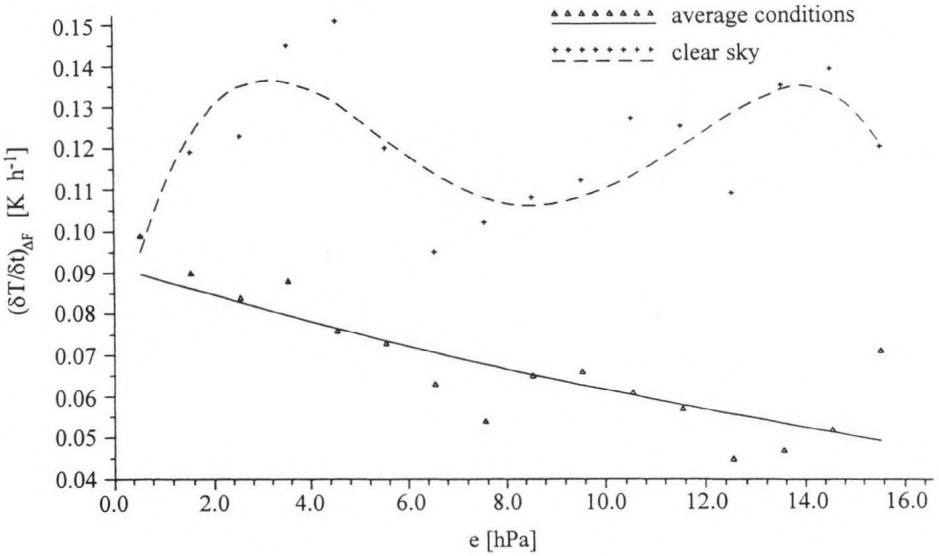

Fig. 7. Dependence of the radiative temperature changes $(\delta T/\delta t)_{\Delta F}$ in K h^{-1} on the water vapor pressure (e) in hPa at the average conditions (exponential curve) as well as at the clear sky (polynomial of degree 4) in the atmospheric layer between Stará Lesná and Skalnaté Pleso during the period 1991–1995.

Analytic expression of the radiative cooling rate dependence on the water vapor pressure at average conditions can be put down in the exponential function

$$\left(\frac{\delta T}{\delta t}\right)_{\Delta F} = 0.0916 \exp(-0.0399 e), \tag{3}$$

with correlation coefficient $r = 0.8527$ between measured and calculated values, while at the clear sky the polynomial of degree 4

$$\left(\frac{\delta T}{\delta t}\right)_{\Delta F} = a_0 + a_1 e + a_2 (e)^2 + a_3 (e)^3 + a_4 (e)^4. \quad (4)$$

The values of the regression coefficients and correlation coefficient are given in *Table 2*.

Table 2. Coefficients a_0, a_1, a_2, a_3, a_4 of Eq. (4), and correlation coefficient (r) between experimental and calculated values

Cloud conditions	Coefficients					
	a_0	a_1	a_2	a_3	a_4	r
Clear sky	-0.0706	0.0516	-0.0131	0.0012	-	0.7566

4. Conclusion

Obtained results have shown that the radiative cooling in the investigated atmospheric layer occurs as a consequence of long-wave radiation emission effect. The most intensive radiative cooling in the layer between Stará Lesná and Skalnaté Pleso was found in December. The most intensive radiative cooling occurs at noon. It was shown that from February to October there is a certain anomaly in the cooling rate values after the sunset. After the sunset the radiative heating is more expressive at mean cloud conditions than at clear sky.

Study of the radiative cooling dependence on the thermal stratification in the atmospheric boundary layer has shown non-linear dependence. The radiation cooling rate increases with the decreasing value of the thermal gradient. The highest values of radiative cooling have occurred at strong thermal inversion and low water vapor pressure. It was confirmed that in annual mean sense, clouds reduce the radiative cooling rate to level of 43% of the value that would exist if skies over measurement sites remained clear.

Acknowledgement–The authors are grateful to the Grant Agency for Science (Grant No. 98/5305/417) for partially supporting this study.

References

Goody, R.M., 1964: *Atmospheric radiation. I. Theoretical basis*. Clarendon Press, Oxford.

Kondratyev, K.Ya., Vulis, I.L., Nikoljskij, G.A. and *Štengelj, M.P.*, 1972: On calculation of the radiative temperature changes in the cloudless atmosphere (in Russian). *Trudy GGO 276*, 196-208.

Kondratyev, K.Ya., 1956: *Radiative heat exchange in the atmosphere* (in Russian). Gidrometeoizdat, Leningrad.

Ostrožlík, M. and *Janičkovičová, L.*, (eds.), 1992–1995: *Results of meteorological measurements at the observatories of the Geophysical Institute of the Slovak Academy of Sciences*. Geophysical Institute of SAS, Bratislava.

Prokofjev, M.A. and *Ter-Markarjanc, N.E.*, 1972: Measurements of radiation in free atmosphere at KENEX expedition (in Russian). *Trudy GGO, 276*, 43-61.

Rodgers, C.D., 1967: The use of emissivity in atmospheric radiation calculations. *Quart. J. Roy. Meteorol. Soc. 93*, 43-54.

Stephens, G.L., Slingo, A., Webb, M.J., Minnett, P.J., Daum, P.H., Kleinman, L., Wittmeyer, I. and *Randall, D.A.*, 1994: Observations of the earth's radiation budget in relation to atmospheric hydrology. 4. Atmospheric column radiative cooling over the world's oceans. *J. Geophys. Res. 99*, 18585-18604.

Timanovskaja, R.G. and *Faraponova, G.P.*, 1967: The radiative heat flux determination in the boundary layer of the atmosphere (in Russian). *Fyzika atmosfery i okeana 12*, 1259-1270.

Zajceva, N.A. and *Šljachov, V.I.*, 1972: On longwave radiation field transformation in the free atmosphere (in Russian). *Trudy GGO 276*, 62-70.

BOOK REVIEW

A. Renoux and *D. Boulaud*: **Les aérosols — Physique et métrologie** (The Aerosols — Physics and Metrology). Lavoisier, Technique et Documentation, Paris, London and New York, 1998. 301 pages, two parts, seven chapters, several figures and tables.

The importance of the study of the atmospheric aerosol is well known for the readers of this journal. Among other things, aerosol particles in the atmosphere influence such basic processes as cloud formation and solar radiation transfer. In this way they play an important role in the control of climate, the most essential ensemble of environmental parameters for human life. Since electric ions and radioactive isotopes are normally attached to fine aerosol particles, the aerosol also determines the electric field and radioactive properties of the air. Less known is, however, that the study of aerosol particles is of interest for different branches of our industrial activity like automobile industry, air cleaning, air conditioning or modern high technology. Further, aerosol science is applied in agricultural practice, e.g. during dispersion of pesticides, herbicides and fertilizers. Finally, the atmospheric aerosol affects our health, while artificial aerosols can be used in medical treatments by inhalation. For this reason, the basic physics and measuring methods of aerocolloidal systems are essential because of many scientific and practical purposes. In this way it is not surprising that several books have been published in this field during the last decades. However, the books available are normally in English language. Thus, the present volume is unique in such a sense that it is prepared for French speaking audience, mainly for students and doctor fellows at French universities.

The first part of the book (physical bases) consists of three chapters written by Prof. A. Renoux. The first chapter summarizes very briefly our knowledge about some basic principles of the atmospheric aerosol. It goes without saying that this is not an easy task. The main merit of this chapter is the short and coherent presentation of the radioactive properties of the atmospheric aerosol. The second chapter is devoted to the size distribution functions used in different aerosol studies as well as to practical methods of their construction. The third chapter is entitled "Physical properties of aerosols". In this important chapter the writer gives an excellent summary of the physical properties of aerosol particles including sedimentation, phoretic forces, coagulation, electric and optical properties as well as condensation and evaporation of liquid particles. The section dealing with the electric properties of aerosol particles can be highlighted in particular. The effects of electric forces are also considered by discussing the coagulation of aerosols and their adherence to a given surface.

The material of this chapter can constitute a good basis of a university course for graduate students. It can also be used by any educated person interested in the field.

The second part of the volume is the work of Prof. D. Boulaud. In three chapters he presents a concise brief survey of measuring methods used to determine the physical properties (number and mass concentration, size distribution etc.) of aerosol particles. In the fourth chapter the reader can learn very easily the basic principles of aerosol measurements including the sampling under different transport conditions. This is a magnificent introduction for the beginners in the field. Chapter 5 is entitled "Instrumental techniques". This is the main chapter of the second part. It contains such important sections as filtration, optical and electric methods as well as sampling by inertial, gravitational and centrifugal forces. Moreover, in this chapter there are two other sections, one is devoted to expansion chambers and diffusion batteries, while the second treats radioactive and piezoelectric procedures of the real time monitoring of the mass concentration. Finally, the last section gives a summary of the generation and measurements of calibration aerosols. The aim of Chapter 6 is to discuss some applications of aerosol measurements at working places and in clean electronic laboratories.

The seventh chapter of the book presents the overall synthesis of the material discussed.

After having read the volume the reviewer concludes that the authors have reached their aim. This not too voluminous book is really a good summary of the physics and metrology of aerosols. It can be used satisfactorily in university practice and it gives a good introduction to the subject. Although it is obvious that this was not in the intention of the authors, it is a pity that the chemistry of aerosols, the chemical composition and chemical identification of atmospheric particles is not discussed. For this reason it seems that an other volume is necessary on aerosol chemistry if the authors want to have a more complete material on aerosols in French. Further, it is recommended to unify in a deeper way the first and second part of the book if it will be reprinted in the future. Thus, literature is given together after the first part, while in the second part it is given separately after each section. In some cases references are not given in a uniform manner. Secondly, some definitions are repeated in the second part which are presented already previously. This is not a problem, but the symbols used in the two parts are sometimes different. Generally speaking, a more careful editing would have increased further the level of the book. The reviewer has to emphasize, however, that these formal points do not touch the technical merits of the book, which can be proposed to everybody who wants to make an acquaintance with the physics and metrology of aerosols in French language.

E. Mészáros

ATMOSPHERIC ENVIRONMENT

an international journal

To promote the distribution of Atmospheric Environment *Időjárás* publishes regularly the contents of this important journal. For further information the interested reader is asked to contact *Prof. P. Brimblecombe*, School for Environmental Sciences, University of East Anglia, Norwich NR4 7TJ, U.K.; E-mail: atmos_env@uea.ac.uk

Volume 32 Number 13 1998

European Scientific Assessment of the Atmospheric Effects of Aircraft Emissions

Volume 32 Number 14/15 1998

Volume 32 Number 16 1998

Volume 32 Number 17 1998

Volume 32 Number 18 1998

Research on the Effects of Aircraft and Spacecraft Upon the Atmosphere

IDŐJÁRÁS

VOLUME 102 * 1998

BUDAPEST, HUNGARY

AUTHOR INDEX

TABLE OF CONTENTS

I. Papers

II. Book review

III. News

Contents of journal Atmospheric Environment, 1998

IV. SUBJECT INDEX

The asterisk denotes book reviews

A

NOTES TO CONTRIBUTORS OF *IDŐJÁRÁS*

The purpose of the journal is to publish papers in any field of meteorology and atmosphere related scientific areas. These may be

- reports on new results of scientific investigations,
- critical review articles summarizing current state of art of a certain topic,
- shorter contributions dealing with a particular question.

Each issue contains "News" and "Book review" sections.

Authors may be of any nationality, but the official language of the journal is English. Papers will be reviewed by unidentified referees.

Manuscripts should be sent to
Editor-in-Chief of IDŐJÁRÁS
P.O. Box 39
H-1675 Budapest, Hungary

in three copies including all illustrations. One set of illustrations has to be of camera ready quality, the other two might be lower quality.

Title part of the paper should contain the concise title, the name(s) of the author(s), the affiliation(s) including postal and E-mail address(es). In case of multiple authors, the cover letter should indicate the corresponding author.

Abstract should follow the title, it contains the purpose, the data and methods as well as the basic conclusion.

Key-words are necessary to help to classify the topic.

The text has to be typed in double spacing with wide margins. Word-processor printing is preferred. The use of SI units are expected. The negative exponent is preferred to solidus. Figures and tables should be consecutively numbered and referred to in the text.

Mathematical formulas are expected to be as simple as possible and numbered in parentheses at the right margin. Non-Latin letters and hand-written symbols should be indicated and explained by making marginal notes in pencil.

Tables should be marked by Arabic numbers and printed in separate sheets together with their captions. Avoid too lengthy or complicated tables.

Figures should be drawn or printed in black and white, without legends, on separate sheets. The legends of figures should be printed as separate list. Good quality laser printings are preferred as master copies.

References: The text citation should contain the name(s) of the author(s) in Italic letter and the year of publication. In case of one author: *Miller* (1989), or if the name of the author cannot be fitted into the text: *(Miller,* 1989); in the case of two authors: *Gamov* and *Cleveland* (1973); if there are more than two authors: *Smith et al.* (1990). When referring to several papers published in the same year by the same author, the year of publication should be followed by letters a,b etc. At the end of the paper the list of references should be arranged alphabetically. For an article: the name(s) of author(s) in Italics, year, title of article, name of journal, volume number (the latter two in Italics) and pages. E.g. *Nathan, K.K.,* 1986: A note on the relationship between photosynthetically active radiation and cloud amount. *Időjárás 90*, 10-13. For a book: the name(s) of author(s), year, title of the book (all in Italics except the year), publisher and place of publication. E.g. *Junge, C. E.,* 1963: *Air Chemistry and Radioactivity*. Academic Press, New York and London.

The final version should be submitted on diskette altogether with one hard copy. Use standard 3.5" or 5.25" DOS formatted diskettes. The preferred word-processors are WordPerfect 5.1 and MS Word 6.0.

Reprints: authors receive 30 reprints free of charge. Additional reprints may be ordered at the authors' expense when sending back the proofs to the Editorial Office.

More information: gmajor@met.hu
Information on the last issues:
http://www.met.hu/firat/ido-e.html

Published by the Hungarian Meteorological Service

Budapest, Hungary

INDEX: 26 361

HU ISSN 0324-6329